

# SANDIA REPORT

SAND99-8200

Unlimited Release

Printed April 1999

## Mechanical Properties of a Metal Powder-Loaded Polyurethane Foam

S. H. Goods, C. L. Neuschwanger, L. L. Whinnery

Prepared by  
Sandia National Laboratories  
Albuquerque, New Mexico 87185 and Livermore, California 94550

Sandia is a multiprogram laboratory operated by Sandia Corporation,  
a Lockheed Martin Company, for the United States Department of  
Energy under Contract DE-AC04-94AL85000.

Approved for public release; further dissemination unlimited.



**Sandia National Laboratories**

Issued by Sandia National Laboratories, operated for the United States Department of Energy by Sandia Corporation.

**NOTICE:** This report was prepared as an account of work sponsored by an agency of the United States Government. Neither the United States Government, nor any agency thereof, nor any of their employees, nor any of their contractors, subcontractors, or their employees, make any warranty, express or implied, or assume any legal liability or responsibility for the accuracy, completeness, or usefulness of any information, apparatus, product, or process disclosed, or represent that its use would not infringe privately owned rights. Reference herein to any specific commercial product, process, or service by trade name, trademark, manufacturer, or otherwise, does not necessarily constitute or imply its endorsement, recommendation, or favoring by the United States Government, any agency thereof, or any of their contractors or subcontractors. The views and opinions expressed herein do not necessarily state or reflect those of the United States Government, any agency thereof, or any of their contractors.

Printed in the United States of America. This report has been reproduced directly from the best available copy.

Available to DOE and DOE contractors from  
Office of Scientific and Technical Information  
P.O. Box 62  
Oak Ridge, TN 37831

Prices available from (615) 576-8401, FTS 626-8401

Available to the public from  
National Technical Information Service  
U.S. Department of Commerce  
5285 Port Royal Rd  
Springfield, VA 22161

NTIS price codes  
Printed copy: A03  
Microfiche copy: A01



SAND 99-8200  
Unlimited Release  
Printed April 1999

## MECHANICAL PROPERTIES OF A METAL POWDER-LOADED POLYURETHANE FOAM

S. H. Goods  
Materials Reliability Department  
Sandia National Laboratories/California

C. L. Neuschwanger  
Hewlett-Packard Company  
Palo Alto, CA 94304-1126

L. L. Whinnery  
Materials Processing Department  
Sandia National Laboratories/California

### ABSTRACT

Quasi-static compression tests have been performed on polyurethane foam specimens. The modulus of the foam exhibited a power-law dependence with respect to density of the form:  $E^* \propto \rho^{*n}$ , where  $n = 1.7$ . The modulus data is well described by a simple geometric model (attributed to the work of Gibson and Ashby) for closed-cell foam in which the stiffness of the foam is governed by the flexure of the cell struts and cell walls. The compressive strength of the foam is also found to follow a power-law behavior with respect to foam density. In this instance, Euler buckling is used to rationalize the density dependence.

The modulus of the polyurethane foam was modified by addition of a gas atomized, spherical aluminum powder. Additions of 30 and 50 weight percent of the powder significantly increased the foam modulus. However, there were only slight increases in modulus with 5 and 10 weight percent additions of the metal powder. Strength was also slightly increased at high loading fractions of powder. This increase in modulus and strength could be predicted by combining the above geometric model with a well-known model describing the effect on modulus of a rigid dispersoid in a compliant matrix.

# CONTENTS

Abstract	3
I. Introduction	5
Polyurethane Foams	7
II. Experimental	9
Formulation, Processing and Fabrication of CRETE Specimens	9
Characterization of the Al Powder	10
Formulation and Processing of Al-filled CRETE Foam	10
Scanning Electron Microscopy	11
Mechanical Testing	12
III. Results	5
Microscopy of Unfilled CRETE	13
Mechanical Testing of Unfilled CRETE	15
Microscopy of Al-Loaded CRETE	20
Mechanical Testing of Al-Filled CRETE	22
IV. Discussion	26
Relationship Between the Structure of Foams and Mechanics of Deflection	26
Modulus	26
Collapse Stress	31
Prediction of Powder-Filled Foam Properties	32
Modulus for Al-Loaded CRETE	34
Collapse Stress for Al-Loaded CRETE	36
V. Conclusion	37
VI. Acknowledgement	38
VII. References	39
Distribution	41

# MECHANICAL PROPERTIES OF A METAL-LOADED POLYURETHANE FOAM

## I. Introduction

Foams are widely used in a variety of applications for the advantages they bring in energy absorption characteristics, thermal properties, and specific strength. Polymeric foams are the most common and, depending on their structure (that is, whether or not the foam is open- or closed-cell), are used in applications involving cushioning, thermal insulation and structural support. The application for which a particular foam is suited also depends on the intrinsic properties of the polymer (which determine whether the foam is flexible or rigid).

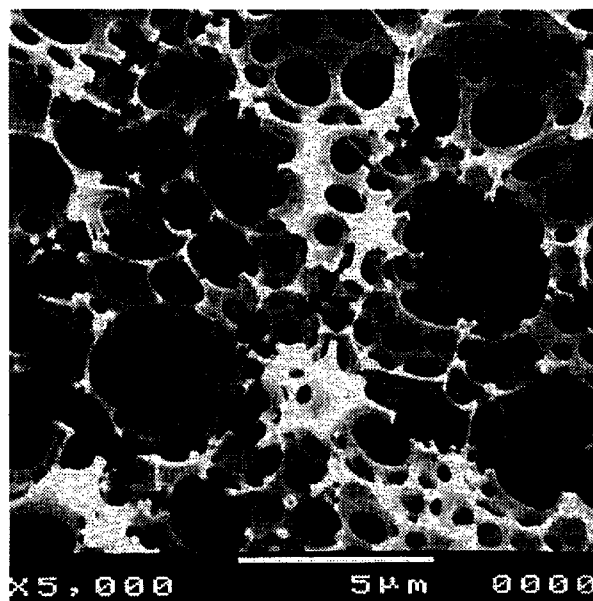
Foams can be considered as cellular solids consisting of two phases: a solid polymer phase, from which the structure of the foam is formed, and a gaseous phase, which may be derived from any of several sources, either physical or chemical. For example, a physically blown foam is processed with a constituent that liberates a gas as the result of a physical process (evaporation or decomposition for example) at either elevated temperatures or reduced pressure [1]. Chemically blown foams are common, and nitrogen and/or carbon dioxide are examples of blowing agents that arise from chemical processes. Carbon dioxide, for instance, can evolve through the reaction of water and an isocyanate. The gas then expands by the application of heat or as the result of the exothermicity of the polymerization reaction.

There are two types of foam structures, open-cell and closed-cell. The chemical composition of the polymer and the conditions under which the polymer is foamed, control the structure of the foam. Open-cell foams invariably start as closed-cell foams, but during the final blowing stages, due either to surface tension or gas pressure, the cell membranes (faces) are destroyed or "roll up" into the cell struts. If solid remains in the cell faces as well as its struts, the final foam is termed closed-cell. Figure 1 illustrates the differences in structure between an open and closed-cell foam. The images shown in Figure 1 are of carbon foams formed by the pyrolysis of cellular polymer precursors [2].

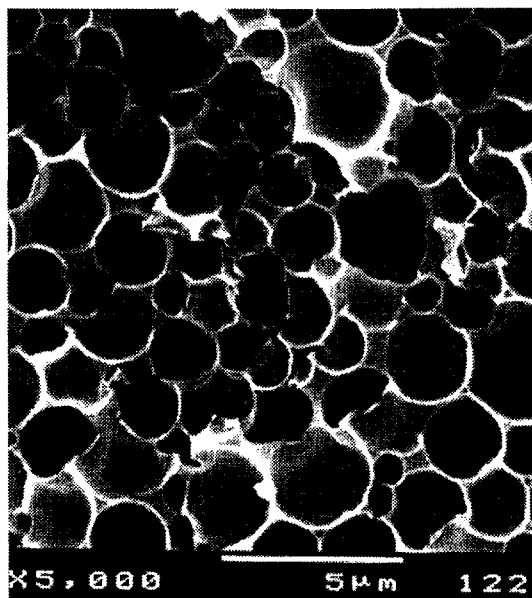
Foams may be flexible or rigid depending on whether their glass transition temperature is above or below room temperature. The glass transition temperature, itself, is dependent on composition, the degree of cross-linking, and crystallinity [1]. In addition, foam structures containing predominately open-cells are more flexible while a structure of mostly closed-cells results in a more rigid foam. The porous and flexible structure of the open-cell foams makes them most suitable for acoustical insulation, furniture and bedding while closed-cell foams are most suited for thermal insulation and structural applications where strength and toughness are important properties.

A foam can also be a composite material incorporating other solids into the host polymer in order to modify certain physical (thermal conductivity or CTE) or mechanical (modulus, strength, toughness) properties [3]. Examples of such additives or fillers include metal powders, glasses

and ceramics. Metal powders or fibers can significantly increase the thermal conductivity of a foam. This can be of advantage when the foam is used as an encapsulant in a storage or shipping container for a component that is self-heating. In such an instance, the ability to tailor the dissipative properties of the foam is important in order to keep the internal temperature of the container acceptably low. It is this interest in modifying the thermal characteristics of a foam through the addition of aluminum powder that originally motivated the current work.



(a)



(b)

Figure 1. Open and closed-cell polymer foams. (a) pyrolyzed polymethacrylonitrile; (b) Resorcinol/Formaldehyde (pyrolyzed).

If a metal-loaded foam is to be used in such an application, the influence of the filler phase on mechanical properties must also be considered since the foam is intended to protect a component from shock or impact. The subject of the present work is the examination of the effect of increasing loading fractions of a 2  $\mu\text{m}$  aluminum powder additive on the modulus and strength of a structural polyurethane (PU) foam. The intrinsic mechanical properties of this foam, called CRETE, have been presented in detail elsewhere [4], and along with additional data, are reviewed here for the sake of completeness.

### Polyurethane Foams

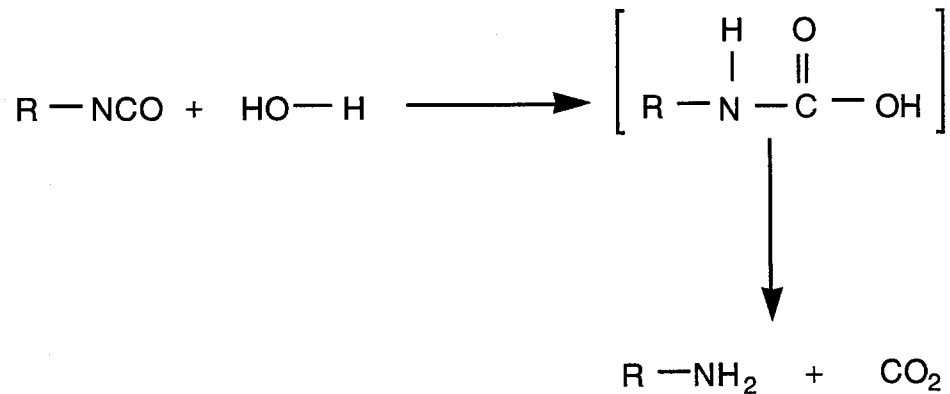
Generally speaking, a polyurethane foam is formed by three principal reactions:

- (1) The reaction of an isocyanate with a hydroxyl on a polyol to produce an urethane:



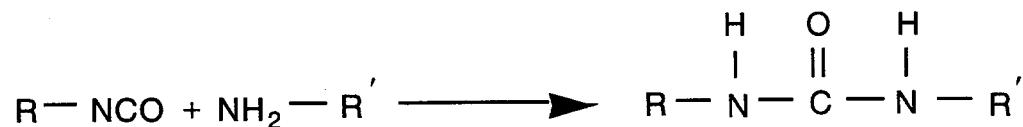
This reaction is also known as the gel reaction.

- (2) The reaction of the isocyanate with water to form an amine:



The carbon dioxide produced during this reaction blows the foam, therefore, this reaction is termed the blow reaction.

- (3) The reaction of the amine with the isocyanate to generate an urea linkage:



These urea linkages are more prevalent in lower density foams where water is used to generate the  $\text{CO}_2$ .

Varying the chemical composition of the starting hydroxyls and isocyanates allows polyurethane foam properties to be changed to meet specific application needs. Early rigid PU foams were based on toluene diisocyanate (TDI) and hydroxyl and carboxyl terminated polyesters. The foam was blown by the reaction of the carboxyl groups with isocyanate and small amounts of water to produce carbon dioxide. The carcinogenic nature of TDI has led to questions regarding both personnel safety and the environmental impact of processing PU foams. In many cases, TDI is now being replaced by alternative isocyanates such as diphenylmethane diisocyanate (MDI) or a modified diphenylmethane diisocyanate (MMDI) [4] as is the case for foam used in this study.

## II. Experimental

### Formulation, Processing and Fabrication of CRETE Specimens

The foam chosen for this study is called CRETE. CRETE is formulated without toluene diisocyanate (TDI) which has been identified a potential human carcinogen. Rather, it incorporates a modified diphenylmethane diisocyanate (MMDI) [4]. It is a rigid, closed cell, water blown polyurethane foam formulated from the following constituents:

#### 1. Voranol 490

A polyether polyol, made from polypropylene oxide and a sucrose/glycerin base, available from Dow Chemical. The manufacturer specifies the following properties:

Density (25 °C)	1.1 g/cm <sup>3</sup>
Typical hydroxyl number	490 mg KOH equiv/g of resin
Functionality	4.3 (calculated)
Average Molecular Weight	460 g/mole
Viscosity (25 °C)	5572 centipoise (cps)

#### 2. DC193

A silicone glycol copolymer surfactant from Air Products with an average hydroxyl number of 75.

#### 3. Polycat 17

A tertiary amine catalyst (trimethyl-N-hydroxyethyl propylene diamine) available from Air Products with an average hydroxyl number of 400.

#### 4. Distilled water

Added in various amounts as a chemical blowing agent producing carbon dioxide. The amount of water added is the determining factor for the foam density as it controls the rise within the foam.

#### 5. Isonate 143L

A modified methylene diisocyanate (MMDI) available from Dow Chemical. The manufacturer specifies the following properties for Isonate 143L:

Isocyanate Equivalent Weight	144.5 g
Content by Weight	29.2 %
Functionality	2.1
Viscosity (25 °C)	33 cps

Components 1-4 are stirred together by hand until thoroughly mixed (approximately 2-4 minutes). The polyurethane foam reaction is then initiated as the isocyanate is added and all of the components are then mixed for one minute using a Conn mixing blade. The mixture is then poured into a non-silicone, waxed, cylindrical mold, covered and sealed with a clamp which is hand tightened. When processed in this fashion, densities higher than free-rise densities can be achieved. Such foams are called "packed" and the packing factor is the ratio of this higher density to the free-rise density. All of the foams presented here were processed with a packing factor of

two. Once the isocyanate is added, the working time for CRETE is approximately eight minutes, but can be adjusted for by varying the amount of catalyst. Working time for the metal-loaded foams can be significantly shorter due to either adsorbed water on the powder or other catalytic effects due to the high surface area of the metal. After the reaction is completed, but before the samples are removed from the mold, they are cured at 66°C for a minimum of four hours. Typical foam formulations are shown in Table I below.

**TABLE I: SELECTED FORMULATIONS FOR FOAM SPECIMENS**

Packed Density (g/cm <sup>3</sup> )	0.17	0.22	0.28	0.34	0.42
Voranol 490	100 phr*	100 phr	100 phr	100 phr	100 phr
DC193	2.53 phr	2.45 phr	2.05 phr	1.90 phr	1.73 phr
Polycat 17	0.50 phr	0.47 phr	0.49 phr	0.54 phr	0.63 phr
Water	1.15 phr	0.78 phr	0.58 phr	0.46 phr	0.34 phr
Isonate 143L	152.2 phr	146.0 phr	142.6 phr	140.5 phr	138.0 phr

\* parts per hundred resin

Right circular cylinders 28.7 mm in diameter and 50.8 mm long are cored from the molded samples with the cylindrical axis parallel to the rise direction of the foam. Care is taken to ensure that the cored samples do not contain any skin or any material from within 3 mm of the surface. The specimen ends are then machined to yield surfaces that are flat and parallel. The final step is to measure the density of each specimen prior to testing.

#### Characterization of the Al Powder

Aluminum powder, 2 μm in diameter, was purchased from Valimet Inc., Stockton, CA. The powder was gas atomized and spherical in shape. A Microtrac® analysis was conducted by Valimet to verify the mean particle size and distribution. The results of this analysis are presented in Figure 2. From Figure 2, it seen that the median particle size is about 2.5 μm and that more than 50 vol.% of the powder consists of spheres between 2 and 4 μm. No powder particles were greater than 12 μm in diameter.

The as-received powder tended to agglomerate. In order to minimize this and insure uniform incorporation in the foam constituents, the powder was sieved using a Ro-Tap Sieve Shaker Model B from Tyler Inc., Mentor, Ohio. Powder, sieved to -100 +200, was collected and the process was repeated. This procedure resulted in powder that was more easily blended with the liquid constituents and in foams that were uniform with respect to powder distribution within the cell walls and struts.

#### Formulation and Processing of Al-Filled CRETE Foam

The powder-loaded CRETE foam was formulated in an analogous manner to the unfilled CRETE foam detailed above. The exception was that the Al powder was added to the formulation after components 1-4 were stirred by hand. The weight percent of filler added to the CRETE formulation was calculated according to the following equation:

$$100 \times \frac{x}{x + \text{tot.}} = \text{wt.}\% \quad (1)$$

where:  $x$  = weight of filler to be added  
 tot. = total weight of all liquid constituents  
 wt. % = desired weight percent of filler present in the composite

The formulation was once again stirred by hand. After the powder was completely wetted, the polyurethane foam reaction was initiated with the addition of the Isonate. The components were mixed for one minute using a Conn mixing blade, poured into the mold and machined similar to the unfilled CRETE foam.

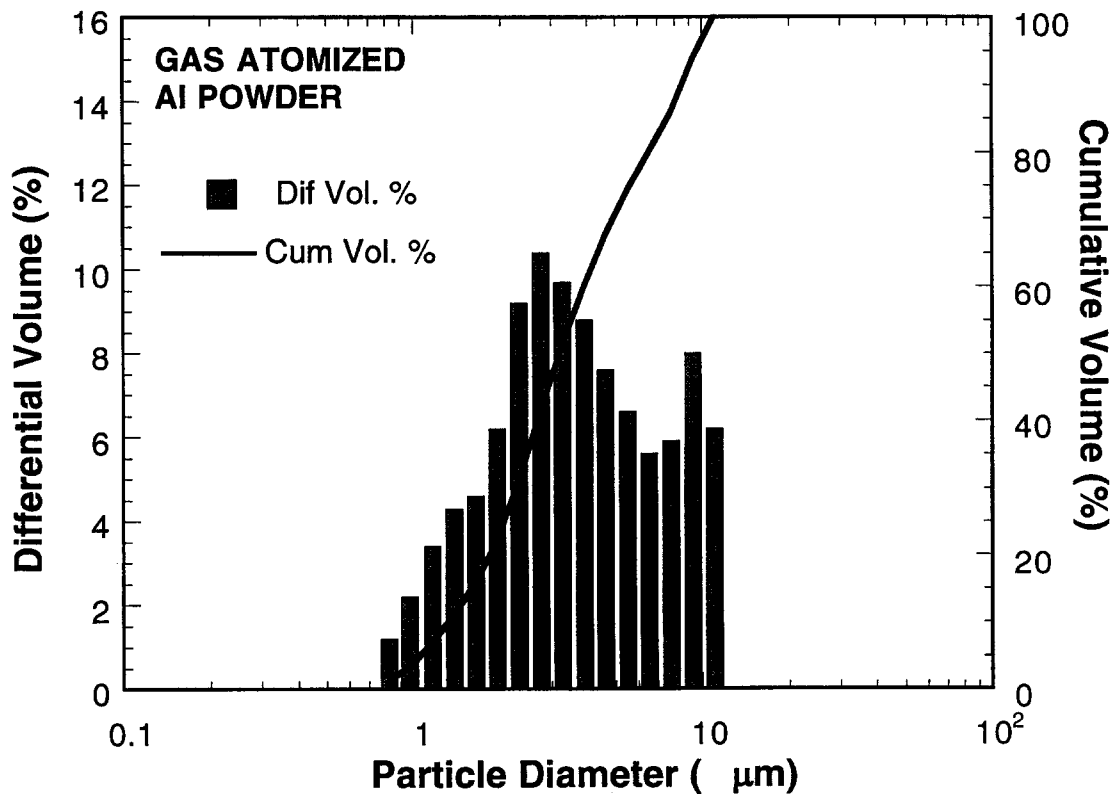


Figure 2. Differential and cumulative volume fractions vs. Al powder diameter.

**Scanning Electron Microscopy**

The structure and morphology of the CRETE and Al-filled CRETE foams were examined using a JEOL 840 scanning electron microscope. Foamed material that remained after the right circular samples were cored, was cut using a bandsaw into small strips and then snapped by hand to reveal a fracture surface. SEM images of the fracture surface were acquired at magnifications between 20X and 2000X in order to characterize the distribution of the metal powder within the foam structure.

### Mechanical Testing

All mechanical testing was conducted under ambient laboratory conditions on specimens ranging in foam density ( $\rho^*$ )<sup>f</sup> from 0.05 g/cm<sup>3</sup> to 0.91 g/cm<sup>3</sup>. The range corresponds to normalized density ( $\rho^*/\rho_{PU}$ ) from 0.04 to 0.76, given a density of solid polyurethane ( $\rho_{PU}$ ) of 1.2 g/cm<sup>3</sup> [5]. Mechanical properties in compression were evaluated on the right cylinders described above using a conventional Instron mechanical test frame. Tests were conducted in displacement control at a constant initial strain rate of  $1.7 \times 10^{-4} \text{ s}^{-1}$ .

Moduli,  $E^*$ , were calculated as the slope of the linear portion of the loading curves. In all instances, a mechanically attached extensometer was used for displacement measurement. The modulus of CRETE measured in tension has been reported in a previous study [4]. Those results are included here for the sake of completeness. Macroscopic failure did not occur under compressive loading for unfilled CRETE specimens and low loading fractions (less than 30 wt. %) of the Al-filled polymers. In these cases, tests were generally run to strains of approximately 0.3. Collapse stress, defined as the stress plateau subsequent to the initial linear loading region, was also characterized as a function of specimen density. The measurement of these mechanical property characteristics is shown schematically in Figure 3.

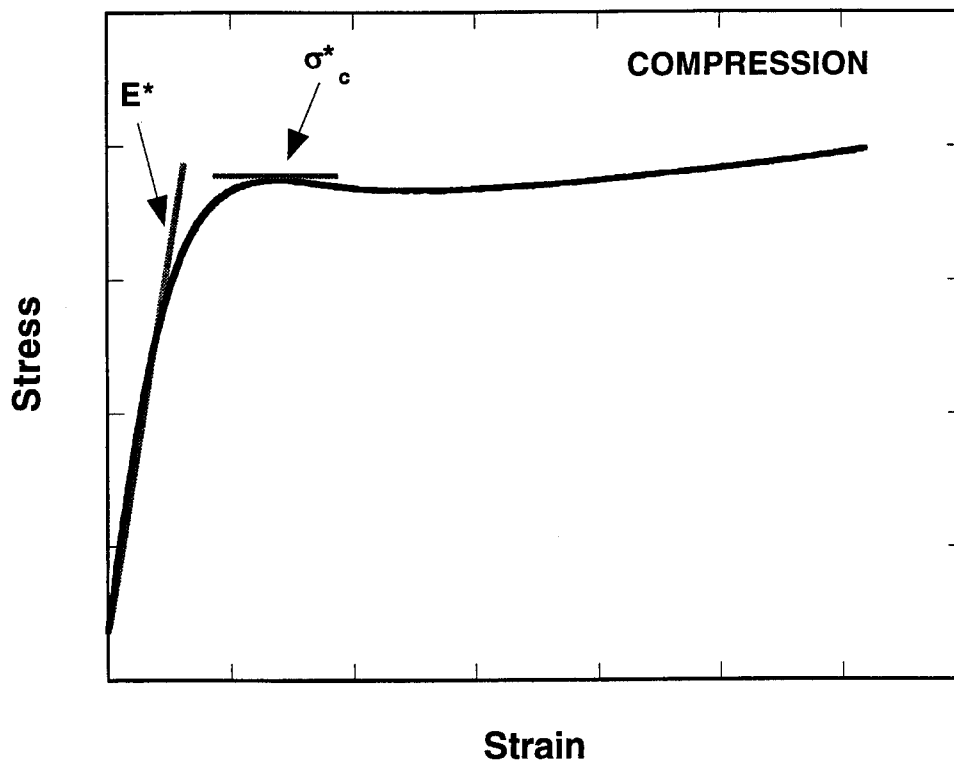


Figure 3. Typical compressive of a polymer-based foam. Modulus is computed on the basis of the initial loading slope while collapse stress is the plateau that follows the initial rapid loading.

<sup>f</sup> terms or values annotated by "\*" refer to parameters of the foam, other terms annotated by "PU" refer to parameters related to the solid polymer.

### III. Results

#### Microscopy of Unfilled CRETE

Scanning electron microscopy was conducted on foam specimens to determine their structure and morphology. Micrographs of CRETE foam at densities of  $0.12 \text{ g/cm}^3$ ,  $0.36 \text{ g/cm}^3$ , and  $0.7 \text{ g/cm}^3$ , are illustrated in Figures 4 (a), (b), and (c), respectively. Fracture surfaces were examined at low magnifications to best illustrate the average foam characteristics. The cell microstructure is quite uniform and the cell diameter can be calculated using a line intercept method [6]. In this fashion, the average cell diameter in Figure 4 (a) was found to be approximately  $700 \mu\text{m}$ . The dimples on the spherical cells represent the areas of contact between adjoining cells. These contact areas are continuous, thin polymer films that form the walls or faces, enclosing the cells. The intersection of three or more cells results in the formation of a cell strut, which is the principal “structural” member of the foam. A representative polymer strut is magnified in the insert in Figure 4 (a) to illustrate this important feature. This high magnification image reveals that the cell walls are very thin, only a few microns in thickness. Thus, the majority of the polymer resides in the struts.

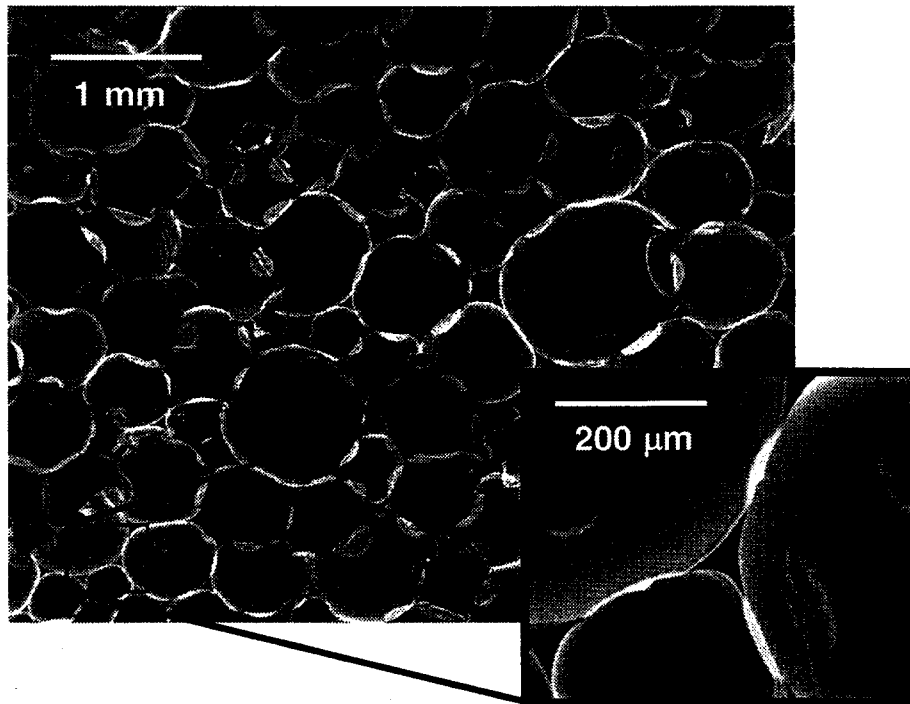


Figure 4 (a). SEM micrograph of CRETE foam,  $\rho^* = 0.12 \text{ g/cm}^3$ . A typical polymer strut is shown in greater detail.

Increasing the CRETE density resulted in smaller cells as illustrated in Figure 4 (b). The structure is still relatively uniform with an average cell diameter of  $250 \mu\text{m}$ . At this higher density the cell membranes are thicker on average than those seen in Figure 4 (a). Consequently, more material resides in the cell walls.

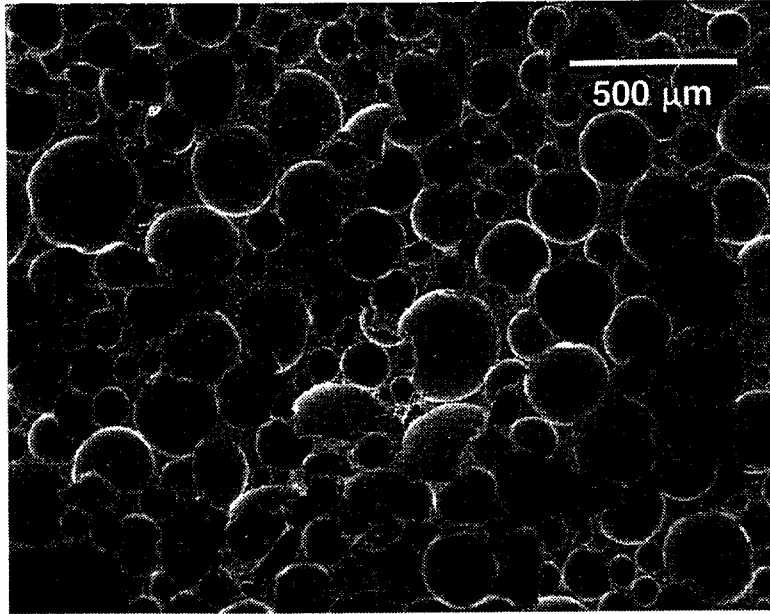


Figure 4 (b). SEM micrograph of CRETE foam,  $\rho^* = 0.36 \text{ g/cm}^3$ .

From Figure 4 (c), it is seen that the cell size has been reduced to approximately  $150 \mu\text{m}$  by doubling the CRETE density to  $0.72 \text{ g/cm}^3$ . In this instance, the microstructure is more representative of solid polyurethane containing voids than it is of a foam. However, it will be shown that even these high density structures can be modeled as foams.

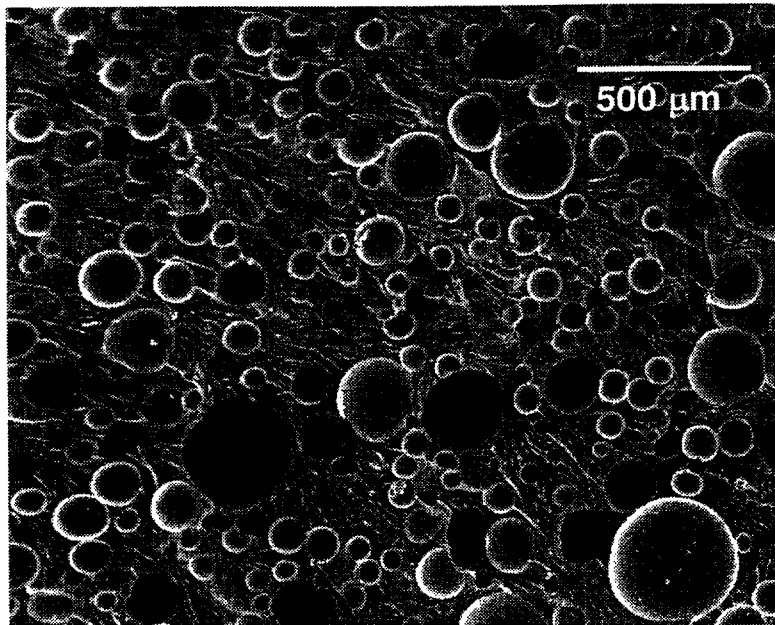


Figure 4 (c) SEM micrograph of CRETE foam,  $\rho^* = 0.72 \text{ g/cm}^3$ .

## Mechanical Testing of Unfilled CRETE

A typical compression test is shown in Figure 5 for a foam having a density of  $0.28 \text{ g/cm}^3$ . In compression, the foam specimens show relatively abrupt yielding followed by a sustained plateau region. At the lower densities the stress after the plateau actually drops, giving rise to a yield point-like behavior. The broad plateau region results from the collapse or cell wall buckling of the foam [7,8]. The stress begins to increase subsequent to this plateau region as the foam begins to densify.

As the CRETE foam is based on polyurethane, its mechanical response to an applied stress or strain is time dependent. This viscoelasticity is what distinguishes the stress-strain response of elastic solids (metals) from that of plastics [8]. The viscoelastic recovery of the polyurethane foam at strains of 0.06 and 0.15 is seen in the inserts to Figure 5. Inset A shows the recovered strain as a function of time for a sample tested to a point near its elastic collapse. Upon unloading, the sample recovers much of the imposed strain instantaneously. Additional strain is recovered over several hours, leaving a permanent plastic strain of less than 1%. Inset B shows the recovered strain as a function of time for a sample tested to a strain of 0.15, well beyond the elastic collapse of the foam. Upon unloading, the sample recovers about half the imposed strain instantaneously. Over several hours, the sample recovers even more strain leaving a "permanent" strain of approximately 0.06. Note that the small, non-linear initial loading regime is simply an experimental artifact.

Unlike the tests performed in tension [4], fracture is inhibited by the absence of far-field tensile stresses and as a result, engineering strains up to 90% have been measured with little observable indication of fracture. Figure 6 shows a series of tests in which specimens were compressed to the maximum capacity of the loading fixtures. None of the specimens shown here exhibited any fracture. From Figure 6, it is seen that low density samples ( $\rho^* < 0.4 \text{ g/cm}^3$ ) exhibit a long plateau region spanning a broad range in strain before the stress starts to rise rapidly. As the foam density increases, the range of the plateau region decreases and densification occurs at smaller strains. For example, a foam density of  $0.17 \text{ g/cm}^3$  has a plateau region spanning a strain of 0.6. In contrast, a sample with a density of  $0.38 \text{ g/cm}^3$  exhibits a plateau stress that spans a strain of 0.35. At yet higher densities, the plateau stress is less well defined. In order to expedite testing, compression strains for tests other than those illustrated in Figure 6, were limited to 0.3, which was sufficient to characterize the modulus and plateau stress values for each specimen.

A comparison between the tension and compression stress-strain responses of CRETE foam having a density of  $0.24 \text{ g/cm}^3$  is shown in Figure 7. Both tests were conducted at the same strain rate. The curves overlay up until the point of tensile failure, suggesting that the microstructural processes governing elastic deformation and the low strain response in both tension and compression are identical.

Moduli, derived from the compression tests, as a function of foam density are shown in Figure 8. In this figure, the moduli derived from tension testing [4] are also included. The compression testing yields the same moduli as tension.

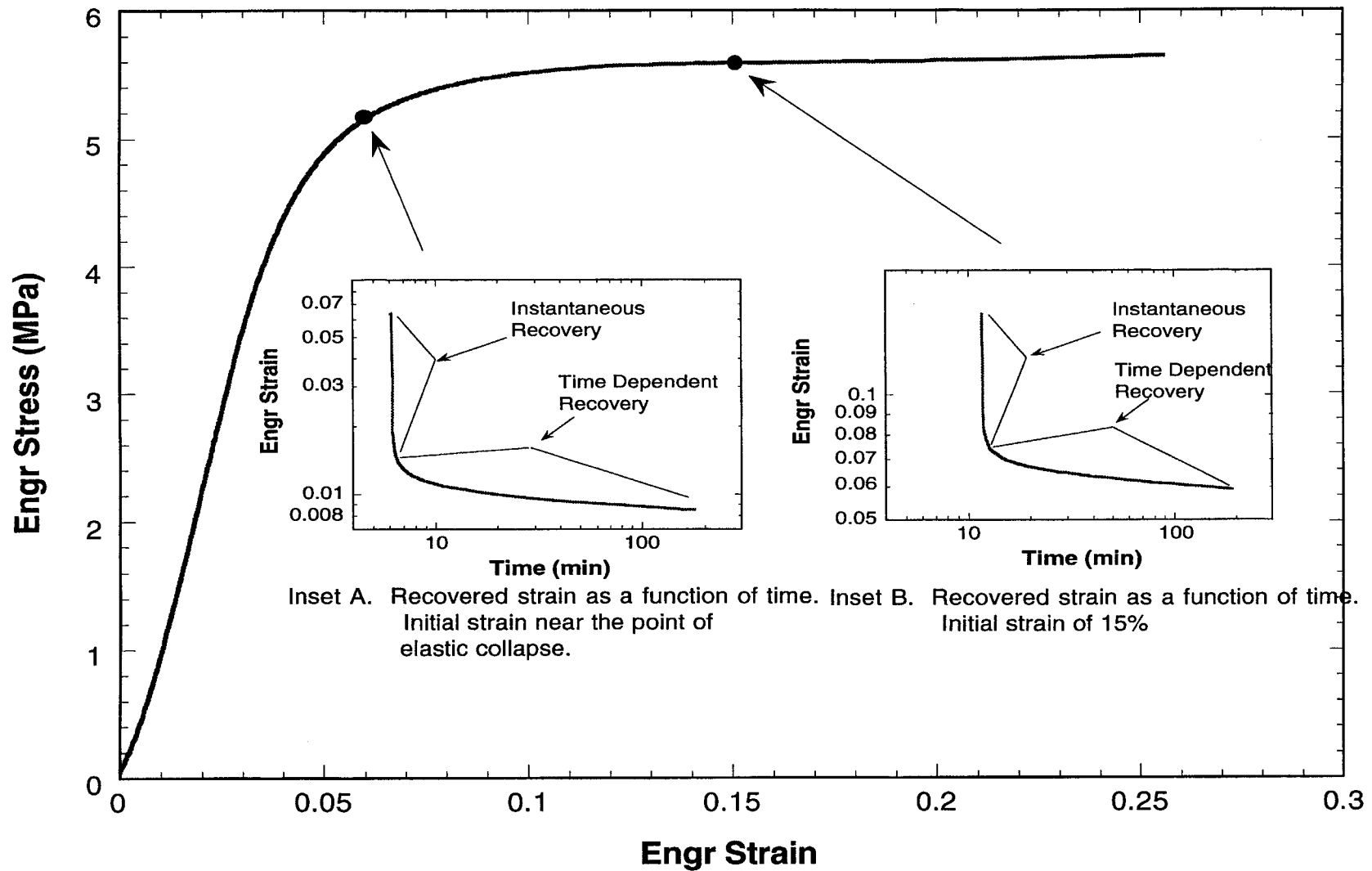


Figure 5. Compression test results for a foam,  $\rho^* = 0.28 \text{ g/cm}^3$ . An abrupt yield point is followed by a sustained plateau region. Insets A and B show recovered strain as a function of time for initial strains of 0.06 and 0.

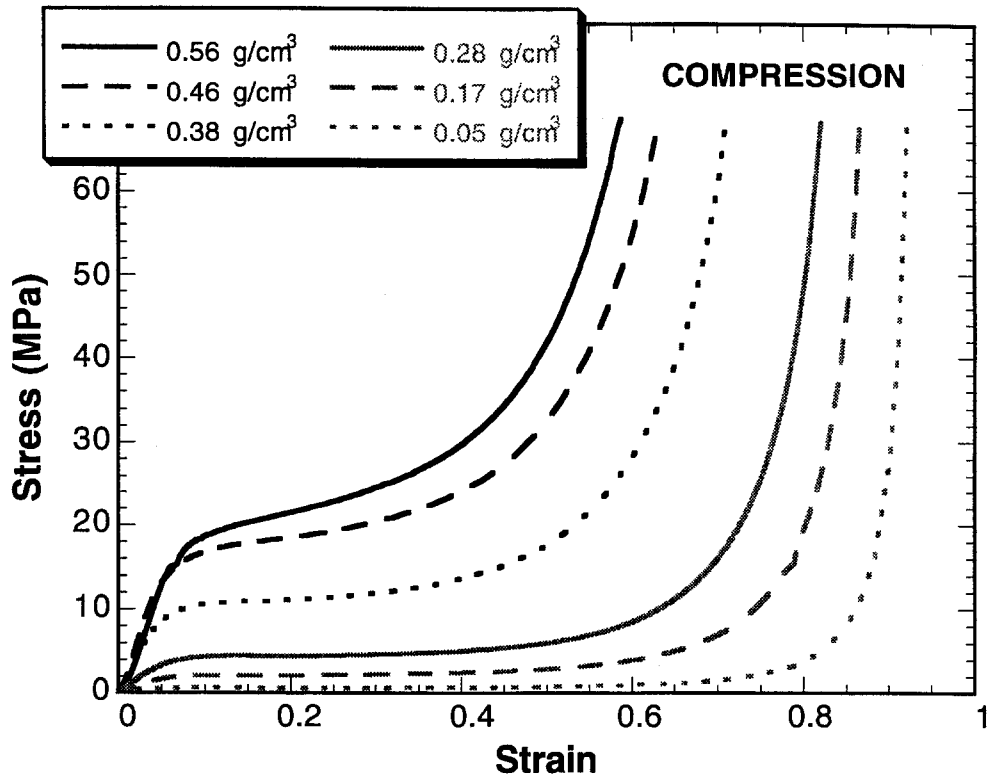


Figure 6. Compression stress strain curves over a range of foam densities. Strains up to 90% are observed without any indication of fracture in the specimens.

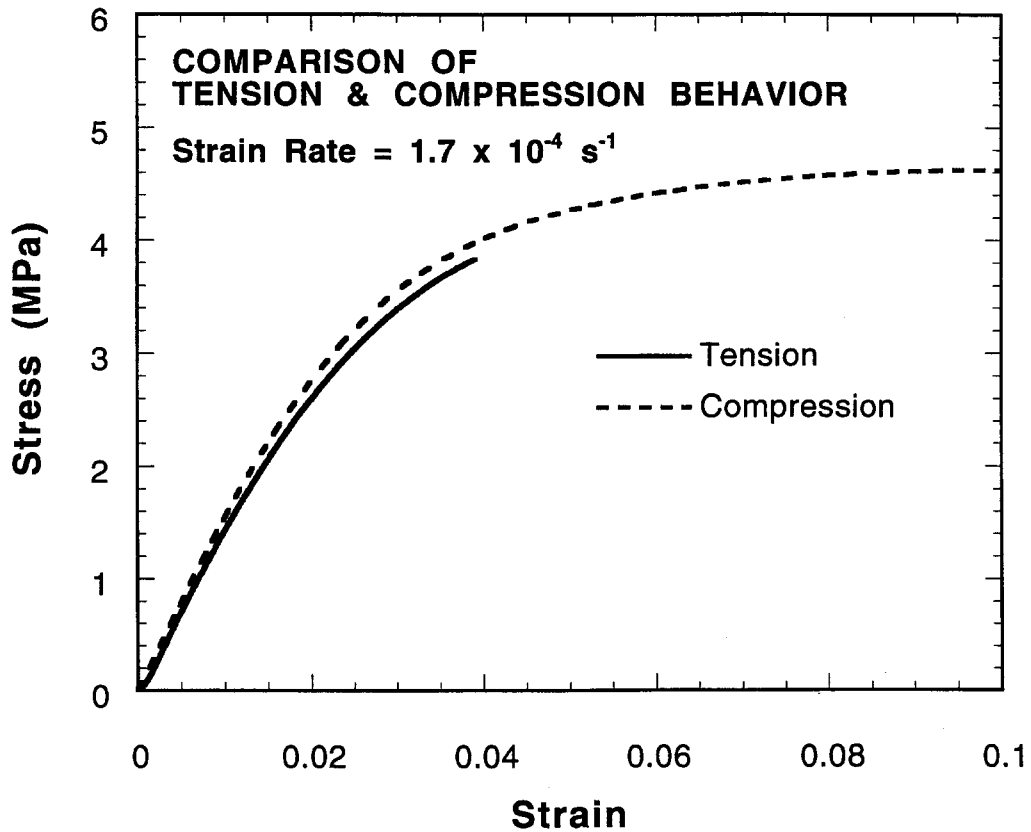


Figure 7. Tension and compression behavior for foam specimens of the same density (0.24 g/cm<sup>3</sup>).

All of the data can be fit with a power-law expression with respect to density of the form:

$$E^* \propto (\rho^*)^n \quad (2)$$

where  $E^*$  is the modulus of the foam,  $\rho^*$  is the foam density, and  $n$  is the density exponent. Over the range of density shown in Figure 8, the data are well fit for a density exponent of  $n = 1.7$ . In our earlier study [4], this value of this density exponent was reported as 1.6. With the additional data gathered for the present work, the data is better fit with the revised value of 1.7.

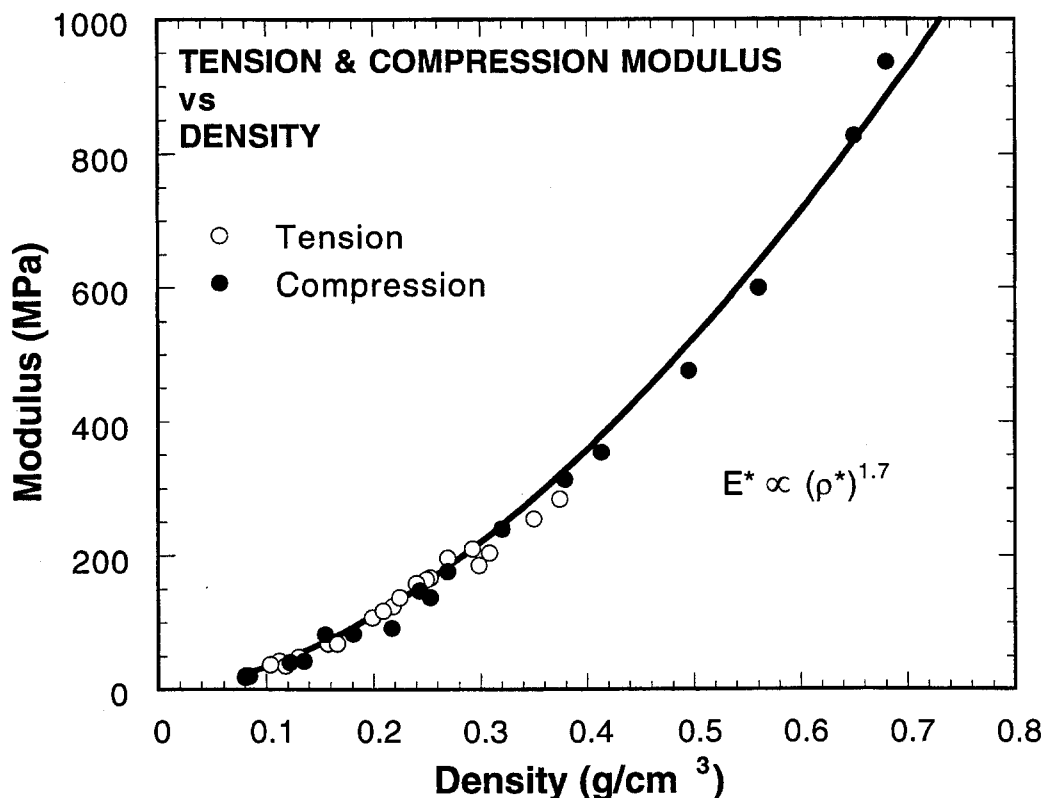


Figure 8. Density dependence of the modulus in tension and compression.

Figure 9 shows the same data plotted on a log-log scale with the density normalized to that of the solid polymer,  $1.2 \text{ g/cm}^3$ . Here the data falls on a straight line with a slope of 1.7, confirming the power-law behavior. The intersection of the best-fit curve and the ordinate for  $\rho^*/\rho_{\text{PU}} = 1$  can be taken to be the modulus of the solid polymer. By doing so we arrive at a value of the solid modulus of 2.5 GPa. This is within the range of reported values for  $E_{\text{PU}}$  of 1.6 to 2.7 GPa [5, 9].

The plateau stress for the foam specimens as function of density is shown in Figure 10. This plateau stress, also called the collapse stress,  $\sigma_c^*$ , is important in the design of cushions for shock or impact mitigation because it represents the onset of the mechanical instability of the foam microstructure [7,8]. It too, exhibits a power-law dependence with respect to foam density although the density exponent, 2.1, is somewhat higher than that exhibited by the modulus. This

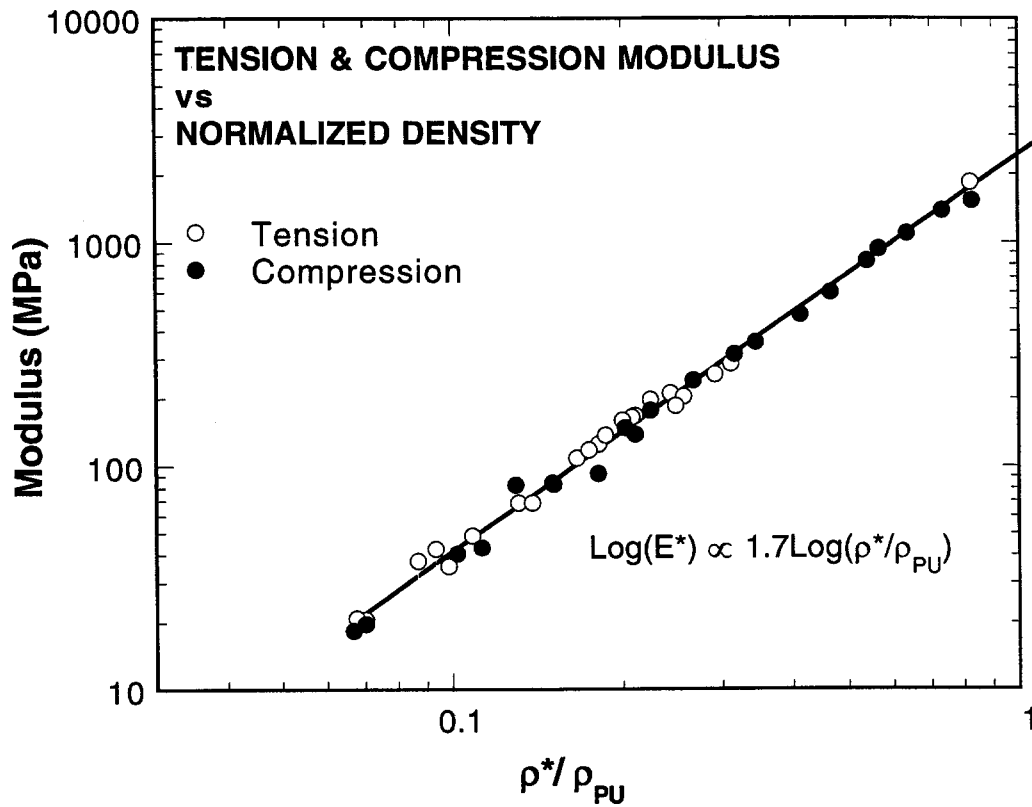


Figure 9. Log-log plot showing power-law behavior between modulus and normalized density.

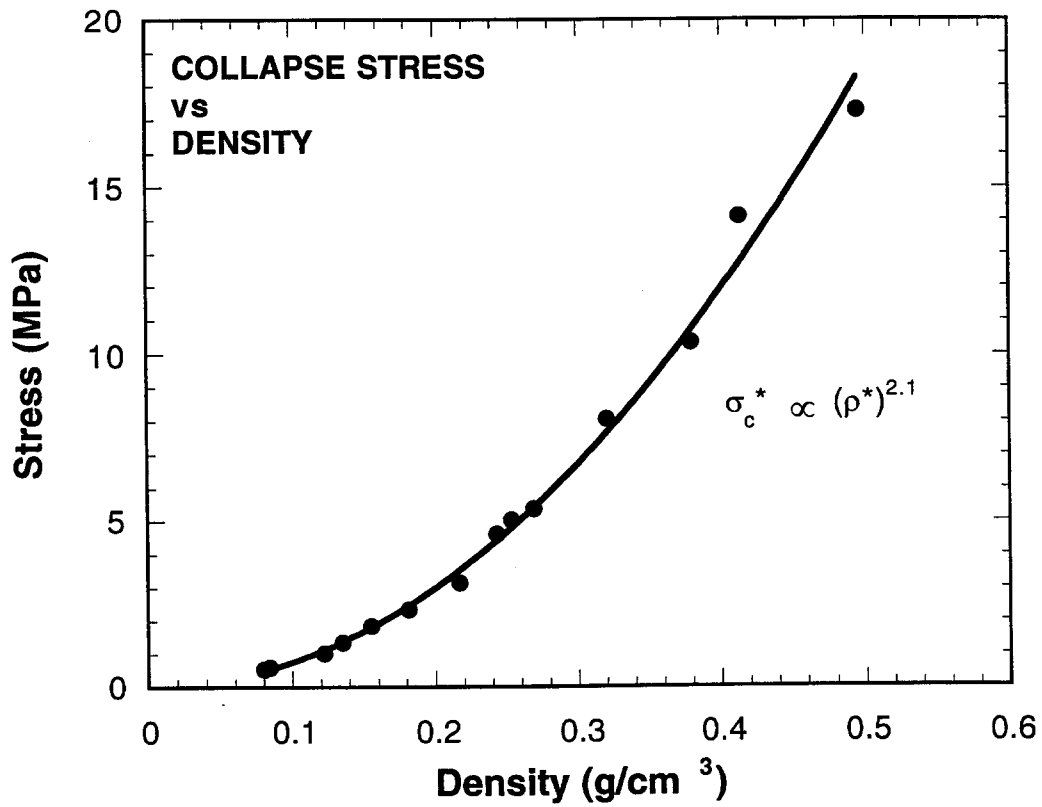


Figure 10. Power-law dependence of the collapse stress.

relationship is shown on a log-log scale in Figure 11. As with Figure 9, the data fall on a straight line, although here the slope equals 2.1.

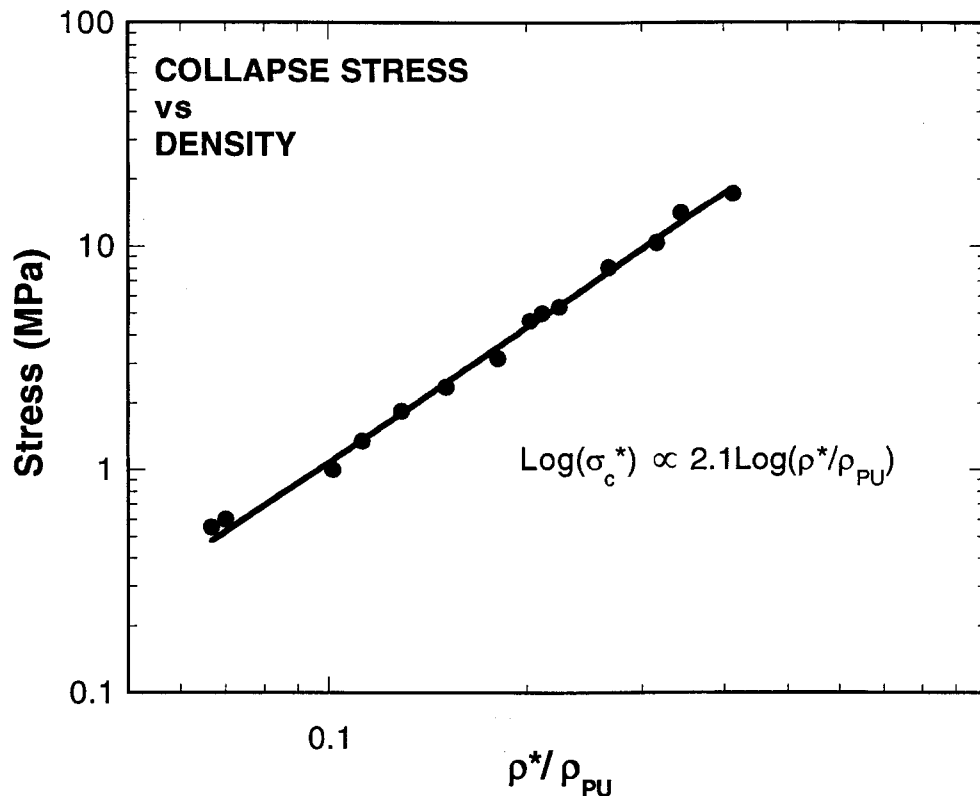


Figure 11. Log-log plot showing power-law behavior between collapse stress and normalized density.

### Microscopy of Al-Loaded CRETE

SEM analysis of the microstructure of the Al-filled foam revealed that overall, the morphology of the cell structure was unaffected by the presence of the Al powder. That is, for any given foam density, the size and shape of the cells were the same for the loaded foams compared to the unloaded foams. At high magnifications, a uniform distribution of aluminum particles is found throughout the foam struts and cell walls of the foam. Figure 12 (a), (b) and (c) are scanning electron micrographs of the fracture surfaces of three Al-loaded specimens having a constant foam density of  $0.28 \text{ g/cm}^3 \pm 0.01$  and with increasing concentration of aluminum powder (5 wt. %, 10 wt. %, 30 wt. % respectively). In each instance, a single strut is isolated to highlight the distribution of the aluminum powder. The solid polymer struts are bounded by concave foam cells. With a concentration of only 5 wt. %, it is seen in Figure 12 (a) that the aluminum powder particles are widely separated. Increasing the fraction of aluminum to 10% yields a somewhat higher density of particles within the struts and cell walls as shown in Figure 12 (b). It is also apparent that a number of powder particles have pulled out of the polymer upon fracture leaving behind small dimples. Figure 12 (c) shows the typical distribution of Al powder in a strut at 30 wt.%. The faint features decorating the cell faces are Al particles that reside just below the free surfaces of the cell.

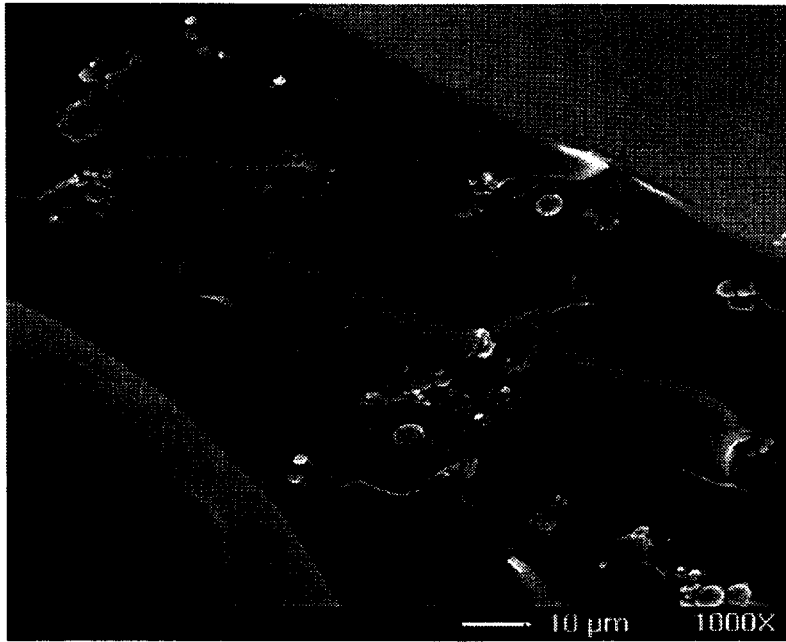


Figure 12 (a). Foam specimen ( $0.29 \text{ g/cm}^3$ ) containing 5 wt. % Al. At this low loading the aluminum powder particles occupy only a small volume fraction of the strut.

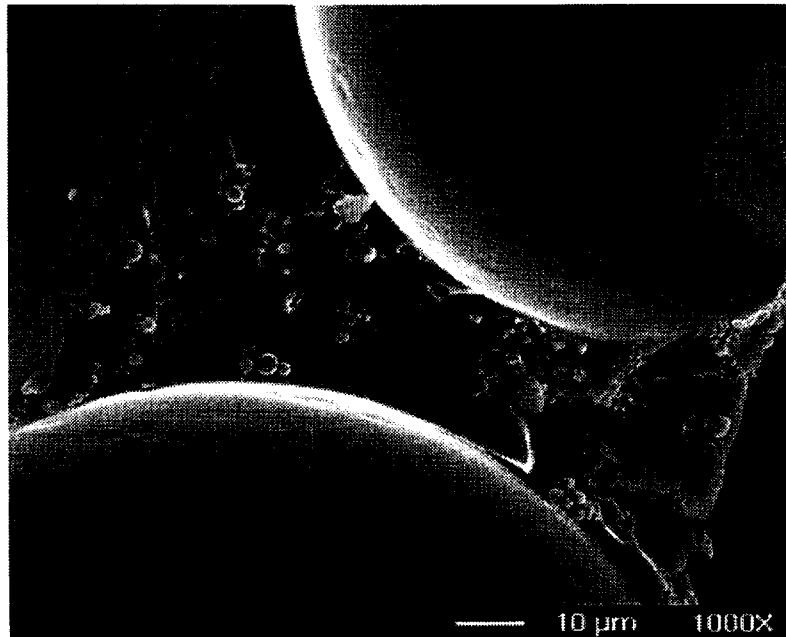


Figure 12 (b). Foam specimen ( $0.28 \text{ g/cm}^3$ ) containing 10 wt. % Al. Along with the higher concentration of powder particles, dimples are visible. These features arise from the debonding of the powder from the polymer strut.

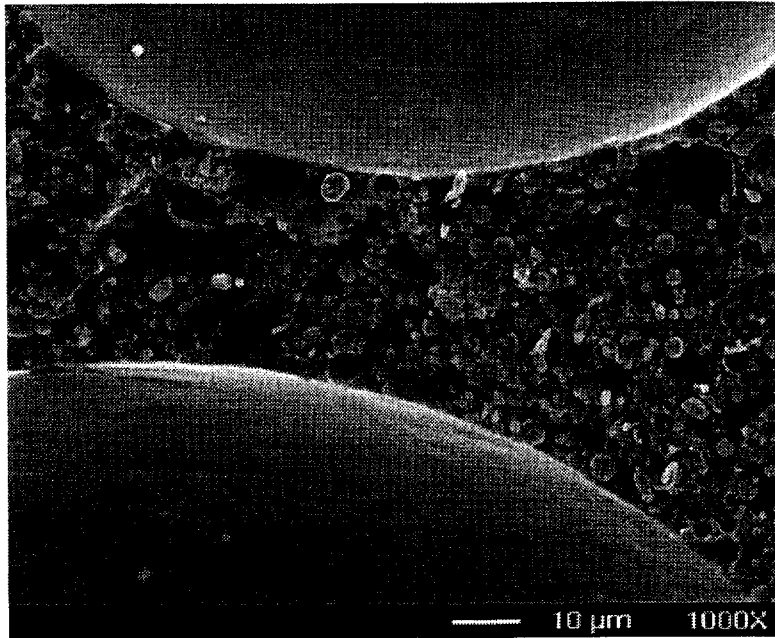


Figure 12 (c). Foam specimen ( $0.29\text{g/cm}^3$ ) containing 30 wt. % Al. A large amount of particles are seen randomly distributed within the strut and the cell walls.

### Mechanical Testing of Al-Filled CRETE

In order to directly observe the influence of the aluminum additive on the mechanical properties of the unfilled CRETE, a common reference state must be established. We choose to compare behavior between the unfilled and Al-filled foam on the basis of polymer foam density. For the case of the filled foams, the polymer foam density is calculated from the measured aggregate density of the specimen and the weight fraction of the aluminum added. Knowing the aggregate density of the filled foam along with the density of aluminum and the weight percent of the aluminum added, the polymer foam density can be calculated. The following example illustrates the method for specimens having an aggregate density of  $0.68\text{ g/cm}^3$  and containing 10 wt. % Al.

For a specimen having:

$$\text{aggregate density} = 0.68\text{ g/cm}^3$$

with:

$$10\text{ wt. \% of Al powder}$$

the volume of Al per unit mass of specimen:

$$\text{vol. Al/g specimen} = \frac{\left(\frac{0.1\text{ g}}{2.7\text{ g/cm}^3}\right)}{\text{g}} = 0.037\left(\frac{\text{cm}^3}{\text{g}}\right) \quad (3a)$$

(density of aluminum =  $2.7\text{ g/cm}^3$ )

the volume of polymer per unit mass of specimen:

$$\text{vol. polymer/g specimen} = \frac{\left(\frac{0.9 \text{ g}}{x \text{ g/cm}^3}\right)}{\text{g}} = \frac{0.9}{x} \left(\frac{\text{cm}^3}{\text{g}}\right) \quad (3b)$$

total volume per unit mass of specimen:

$$\text{total vol./g specimen} = 0.037 \left(\frac{\text{cm}^3}{\text{g}}\right) + \frac{0.9}{x} \left(\frac{\text{cm}^3}{\text{g}}\right) \quad (3c)$$

Since the measured density of the specimen is  $0.68 \text{ g/cm}^3$ :

$$\frac{1}{0.68} \left(\frac{\text{cm}^3}{\text{g}}\right) = 0.037 \left(\frac{\text{cm}^3}{\text{g}}\right) + \frac{0.9}{x} \left(\frac{\text{cm}^3}{\text{g}}\right) \quad (3d)$$

$$\text{polymer foam density} = 0.63 \text{ g/cm}^3.$$

With this basis of comparison, the influence of the Al powder mechanical properties is readily seen in Figure 13. This figure shows a series of compression stress-strain curves for loaded specimens having a constant polymer density of  $0.28 \text{ g/cm}^3$ . It is clear from Figure 13 that progressively increasing the fraction of powder in a foam of constant polymer density increases both the elastic modulus and the strength of the foam. The loaded specimens have moduli that are greater than that of the unloaded CRETE. The magnitude of the increase is dependent upon the amount of filler added. Additions of 5 and 10 weight percent have a small effect on modulus. In the examples shown in Figure 13, 5 and 10 weight percent additions of powder are found to increase the modulus from 175 MPa to 190 and 206 MPa, respectively. The modulus of the foam specimen containing 30 weight percent filler exhibits a modulus of approximately 280 MPa.

The collapse stress of the unfilled CRETE foam was 5.3 MPa, the 5 and 10 weight percent additions of aluminum increased  $\sigma_c^*$ , to 6.0 and 6.4 MPa, respectively. It is also seen from Figure 13 that at 30 weight percent Al, the strength of the foam is about 25% greater than that of the unloaded foam, 8.3 MPa. However, the sample fails at a strain of 0.13 (for the other specimens, the tests were terminated prior to failure at about strains of about 0.25). Unlike the unloaded CRETE or specimens with low loading fractions, this specimen showed evidence of cracking with increasing strain. Such cracking at low strains is uncharacteristic of polyurethane foams of this density and is caused by the incomplete bonding of the Al powder to the polymer matrix. Thus, while the powder may act to strengthen the foam, the individual particles can act as pre-existing defect sites and at high enough concentrations, can allow for easier crack initiation and propagation. At low concentrations, ductility is largely unaffected.

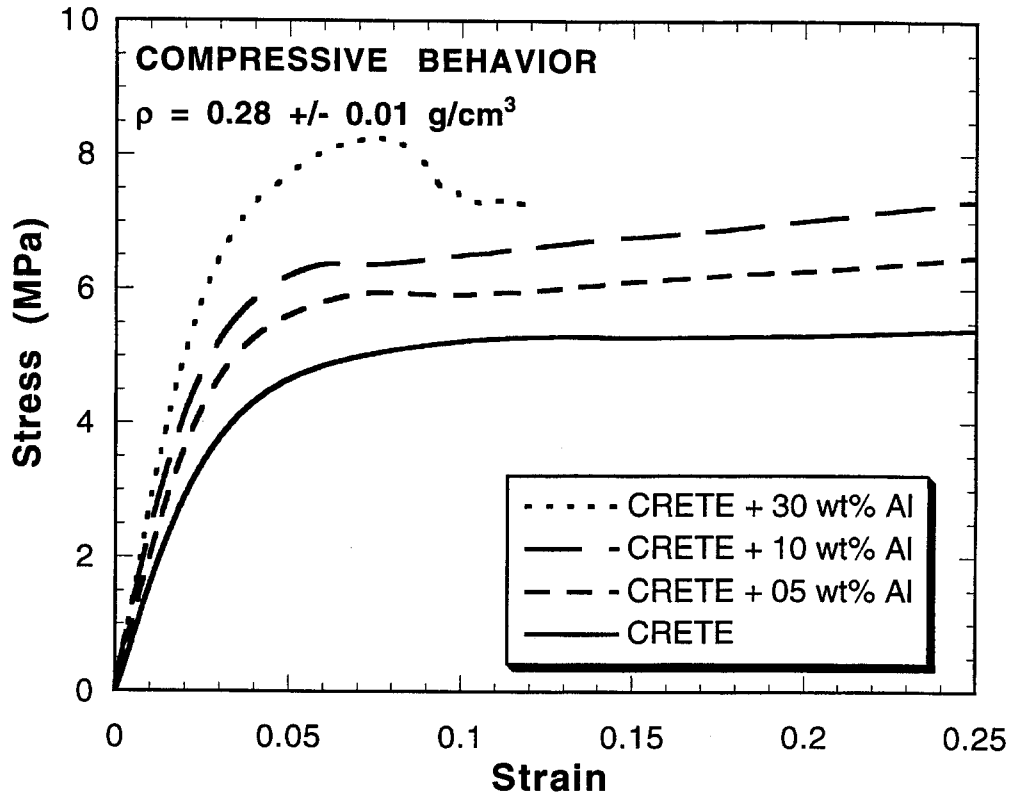


Figure 13. Comparison of the compressive behavior of the Al filled CRETE to the unfilled CRETE foams.

The influence of the rigid filler phase on the modulus of the foam over a wide range of polymer density is shown in Figure 14. This figure compares the original modulus data for CRETE shown in Figure 8 to specimens containing controlled additions of the aluminum powder filler. The abscissa is the back calculated polymer density as was described at the beginning of this section. The solid line represents a best fit through the unfilled CRETE data previously presented in Figure 8. The corresponding data points are omitted for clarity. The measured moduli for the specimens containing 5 wt. %, 10 wt. %, 30 wt. % and 50 wt. % are also shown in this figure. From Figure 14 it is seen that the moduli of the loaded specimens tends to group by loading fraction of aluminum. It is also seen that the power-law dependence,  $n = 1.7$ , denoted by the traces through each set of data still describes the density dependence of the modulus for each loading fraction of aluminum.

It is clear from Figure 14 that aluminum loadings of 5 and 10 weight percent have only a small effect on the modulus of the foam. It is only at the higher loading fractions of 30 and 50 weight percent that a measurable increase in modulus is realized. For example, at relatively low polymer densities ( $\rho = 0.3 \text{ g/cm}^3$ ), the modulus of the loaded foams can be more than doubled by the addition of 50 weight percent Al powder.

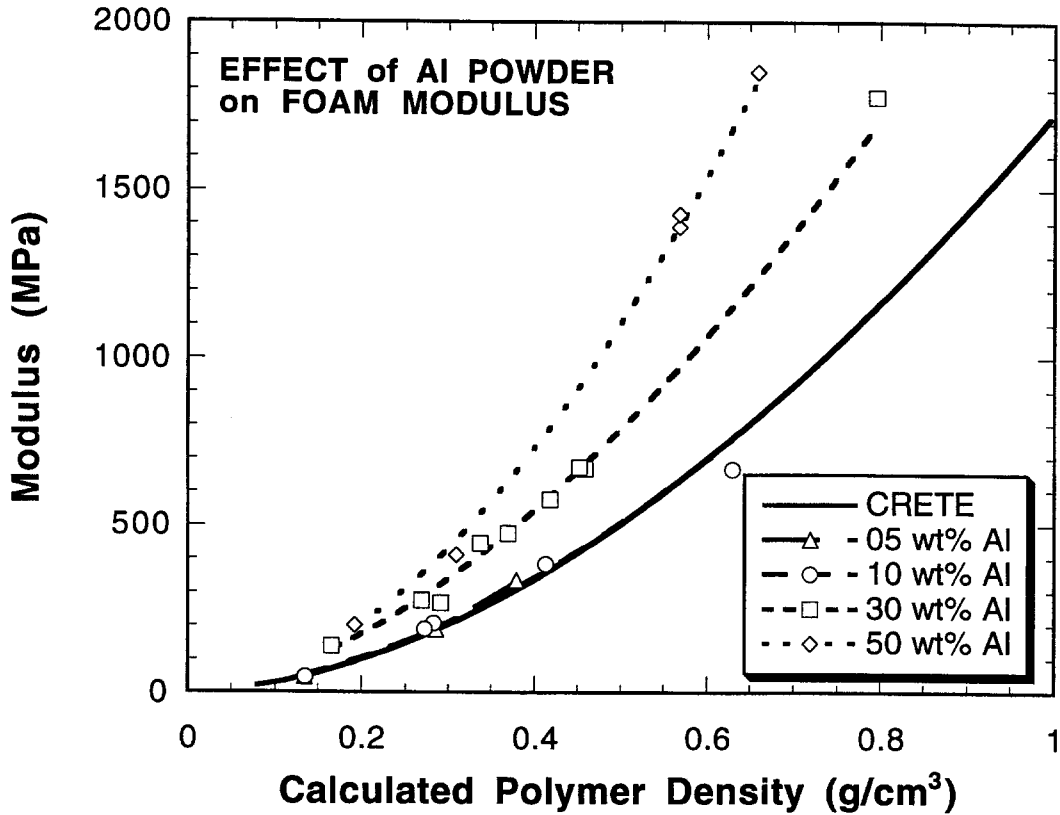


Figure 14. Influence of Al powder additions on the CRETE modulus. Modulus increases with Al concentration and still exhibits the 1.7 power law dependence on density. The solid line represents the best fit through the data in Figure 8.

That the modulus of the foam is found to increase at powder concentration greater than 30% is not unexpected. The effect may be attributed to the formation of a nearly continuous network of aluminum powder at these higher loading fractions since the average number of contacts each particle will have depends on its coordination number and hence the volume fraction of filler in the matrix. For a random dispersion of spherical particles, it has been shown that a continuous network is formed at the critical volume fraction of 0.3 [3]. This volume fraction corresponds to an aluminum content of approximately 50 wt.%, about where the most significant increase in foam modulus was observed.

## IV. Discussion

### Relationship Between the Structure of Foams and Mechanics of Deflection

The dependence of both the modulus and the elastic collapse stress of a polymer foam can be understood in terms of the mechanical properties of the polymer material from which the cell struts (and in the present case, the cell walls) are made and the deformation mechanics of the cellular structure itself. Elastic moduli are related principally to the bending stiffness of the members comprising the cellular structure while the elastic collapse is caused by the elastic buckling of these same members.

For the discussion presented below, the important cell strut/wall properties are the solid polymer density,  $\rho_s$ , and its modulus,  $E_s$ . The important structural features for the analysis of the modulus and the collapse stress are the normalized density of the foam,  $\rho^*/\rho_s$ , (as before,  $\rho^*$  is the density of the foam) and whether or not the cells are open or closed. In this regard a parameter,  $\phi$ , is defined as the fraction of material in the cell struts. For an open-cell foam,  $\phi = 1$ , while for a closed-cell foam, where some of the polymer is in the cell walls, it is less than 1.

### Modulus

Gibson and Ashby [7,8] have put forth a simple model that has been shown to accurately describe the density dependence of the modulus of a foam and we have reviewed their findings in a previous report [4]. In short, Gibson and Ashby describe a cellular solid as an array of cubic cells of length,  $\ell$ , and struts of thickness,  $t$ , as shown in Figure 15. The cells are then staggered so that corners of one cell rest upon the midpoint of adjacent cells. Such a structure neither corresponds to the actual geometric characteristics of a real foam nor can be reproduced to fill space. It does however, capture the critical physical process that govern the deformation processes of a cellular structure. Described in this fashion, each strut that is normal to an applied load ( $F$ ), becomes a point loaded "beam" and the modulus can be calculated from the elastic deflection of a beam of length  $\ell$ , loaded at its mid-point by a load  $F$ , as shown in the figure.

For an open cell foam, where all of the polymer resides in the cell struts, Gibson and Ashby arrive at simple expression for the density dependence of the modulus of a foam:

$$\frac{E^*}{E_s} \approx \left( \frac{\rho^*}{\rho_s} \right)^2 \quad (4)$$

Equation 4 predicts that, at low strains, a parabolic relationship exists between the modulus of the foam and its density. The data in Figures 8 and 14 however, suggests that the power-law exponent is less than 2. This discrepancy can be found in the fact that the polyurethane CRETE is a closed-cell foam rather than an open-cell foam. In deriving Equation 4, it is assumed that all of the material of the foam is found in the struts that define the cells. In a closed-cell foam, some fraction of the polymer resides in the cell walls or faces rather than solely in the struts.

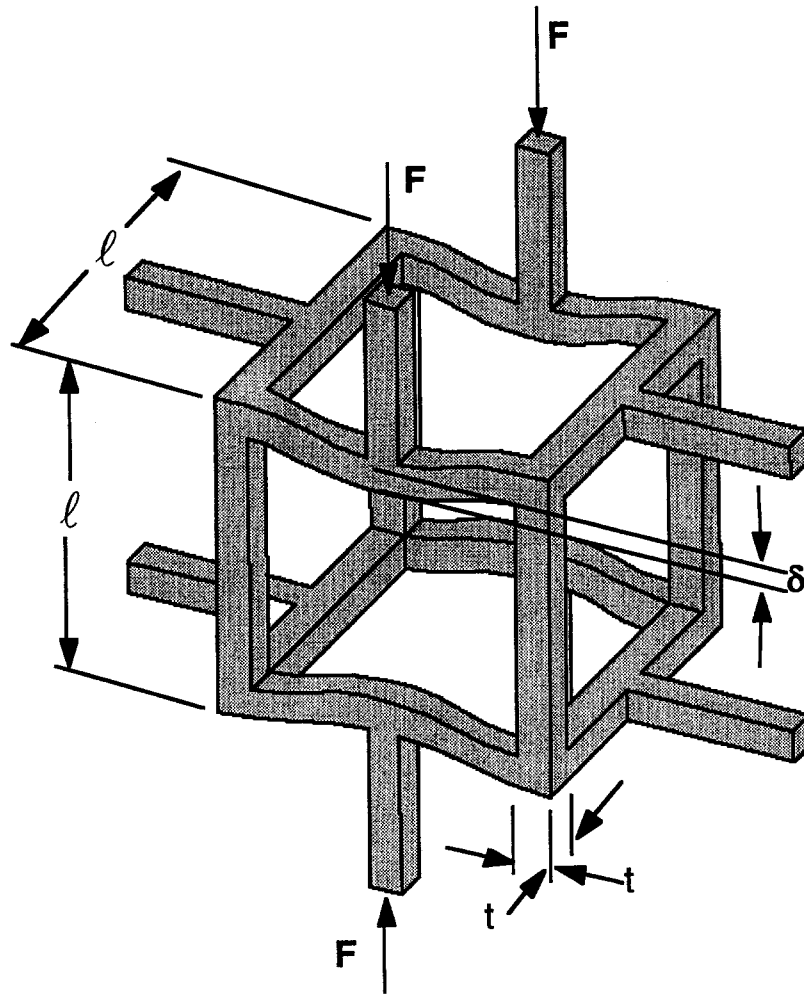


Figure 15. Unit cell shown after deflection of magnitude,  $\delta$ , induced by a force,  $F$ .

Gibson and Ashby represent a closed-cell foam as shown in Figure 16. Here, the fraction of polymer contained in the cell struts having thickness  $t$  is  $\phi$ . The fraction contained in the cell walls of thickness  $t_f$  is  $(1 - \phi)$ . The stiffness of a closed-cell foam (ignoring internal gas pressure) results then from two contributions. The first component is strut bending, as for open-cell foams. The second component arises from the stretching of the cell wall faces [10,11]. Gibson and Ashby [7,8] derive the modulus of a closed-cell foam which accounts for these two components:

$$\frac{E^*}{E_s} \approx \phi^2 \left( \frac{\rho^*}{\rho_s} \right)^2 + (1 - \phi) \left( \frac{\rho^*}{\rho_s} \right) \quad (5)$$

The first term on the right describes the contribution of the cell struts to the modulus while the second term accounts for the stretching of the cell walls. Note that Equation 5 reduces to Equation 4 for  $\phi = 1$  (an open-cell foam). The form of Equation 5 is such that at high relative densities, the

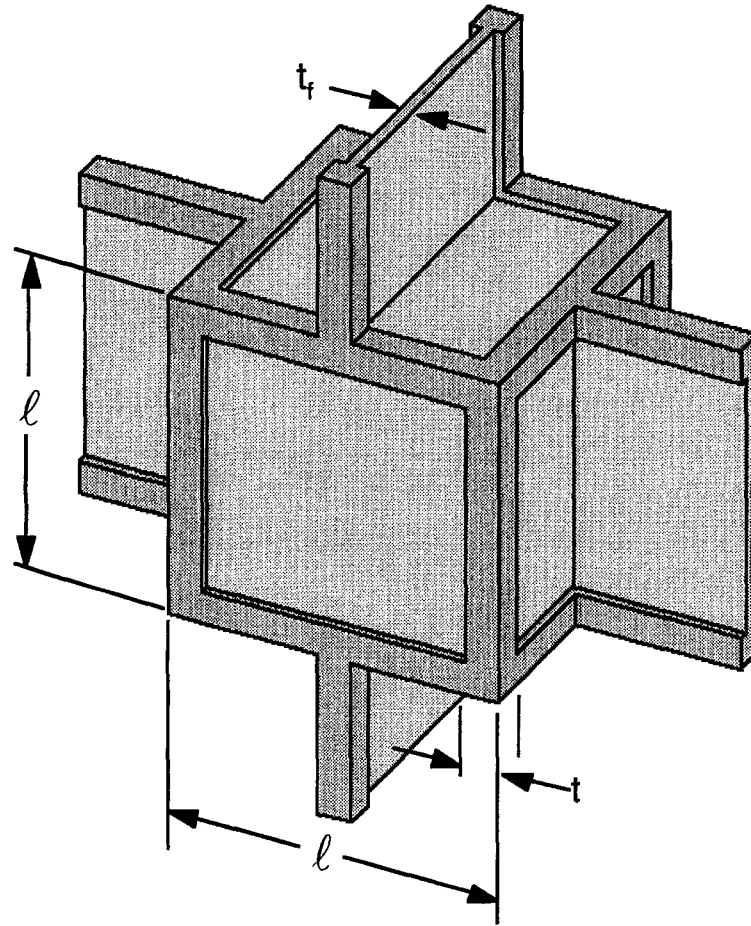


Figure 16. Idealized cell for a closed-cell foam. The cell is comprised of edges or struts of length,  $l$ , and thickness,  $t$ . Cell faces are enclosed by membranes of thickness  $t_f$ .

modulus varies as the square of the density while at low relative densities the modulus is more nearly linearly dependent on the density. Within these density extremes, Equation 5 yields a power-law relationship which can describe the functional dependence of modulus on density with an exponent of 1.7, the value that best fits the data shown in Figure 8.

The data shown in Figure 8 can be quantitatively compared to Equation 5 using known values for  $\rho_s$  and  $E_s$ . For the density of solid polyurethane, we use a value of  $\rho_s = \rho_{PU} = 1.2 \text{ g/cm}^3$  [5]. Since the value for the modulus of solid polyurethane is less well established and varies considerably depending on the precise formulation, processing conditions and product form we use the value obtained from Figure 9,  $E_s = E_{PU} = 2.5 \text{ GPa}$ . This comparison is shown in Figure 17 for  $\phi = 0.9$ . (Note: We have not independently measured  $\phi$  for this foam system, the value used,  $\phi = 0.9$ , is typical for polyurethane foams [12]). Figure 17 shows that the model well represents the data over the range of densities examined experimentally.

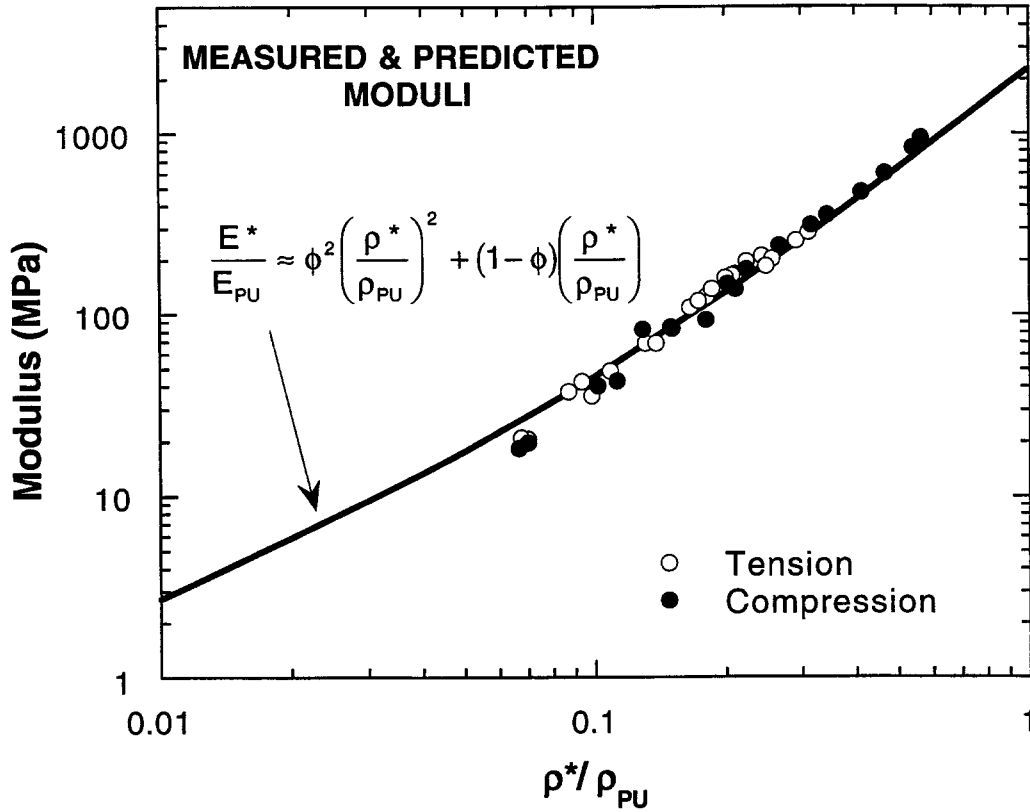


Figure 17. Comparison of modulus measurements to Eq. 5. The density is normalized to the density of the solid polymer 2.5 GPa. The partitioning factor is held constant at  $\phi = 0.9$ .

Equation 5 is also dependent upon the partitioning factor,  $\phi$ . This factor was assumed to be constant over all densities in the previous figure. However, as was seen in Figures 4 (a), (b), and (c), the distribution of polymer within the foam clearly changes with density. At low density the majority of the polymer is associated with the struts and  $\phi = 0.9$  is a reasonable choice. Figures 4 (b), and (c) reveal that with increasing density the thickness of the cell walls increases. Therefore, the partitioning factor must decrease.

The rate at which the partitioning factor decreases with respect to density is not easily determined. To examine the effect of a variable partitioning factor, two empirical expressions were defined that allow  $\phi$  to vary as a function of foam density. These expressions are given as Equations 6a and 6b:

$$\phi = \phi_0 - \left( 0.1 - \left( \frac{\rho^*}{\rho_{PU}} \right) \right)^2 \quad (6a)$$

$$\phi = \phi_0 - \left( 0.1 - \left( \frac{\rho^*}{\rho_{PU}} \right)^{1/2} \right)^2 \quad (6b)$$

The bounding criteria in developing these equations was that at low densities the partitioning factor must approach the literature value (~0.9). In addition, it must change slowly with increasing density to some intermediate value at high densities. As seen in Figure 18, both empirical equations satisfy the imposed boundary conditions. The form of Equation 6a results in a relatively sharp decrease in  $\phi$  at higher densities. In contrast, Equation 6b yields a more gradually decreasing  $\phi$  over a wider range of densities.

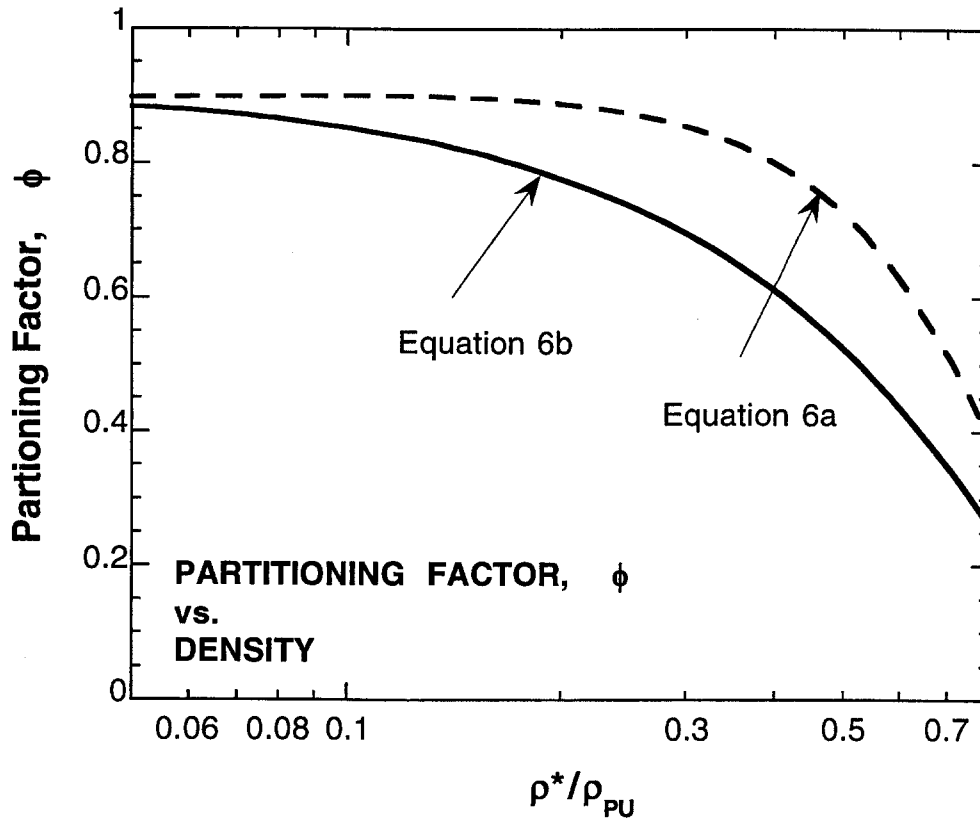


Figure 18. Two empirical equations capturing the behavior of the partitioning factor as a function of normalized foam density.

The effect of a variable partitioning factor on the modulus predicted by Equation 5 is shown in Figure 19. Here the expressions given in Equations 6a and 6b are simply substituted in Equation 5 in place of the constant  $\phi$ . Using Equation 6a results in virtually no change in the predicted modulus. Indeed the new prediction overlays that based on a constant,  $\phi = 0.9$ . Using Equation 6b causes a small increase in the modulus prediction over the normalized density range 0.04 to 0.8. In general, both of the empirical expressions for  $\phi$  exhibit the same trend as that predicted by Equation 5 at a constant,  $\phi = 0.9$ . This suggests that the partitioning factor does not have a strong effect on the density dependence of the modulus over the range of densities examined in the current work.

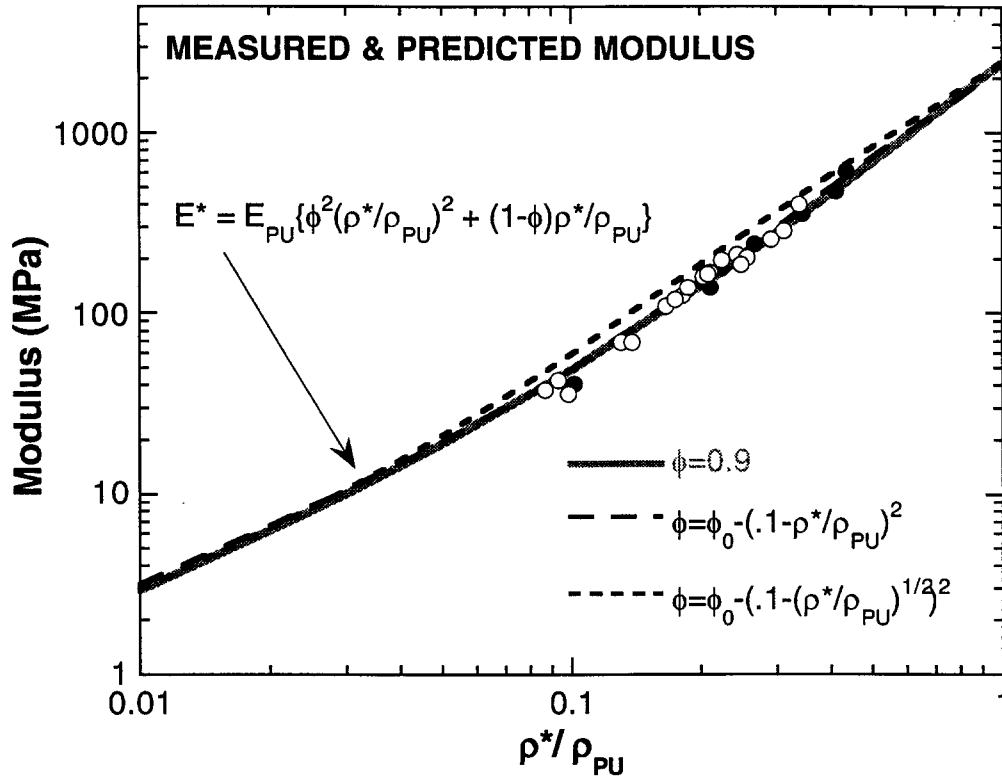


Figure 19. Comparison of the modulus versus normalized density behavior of the two empirical equations for  $\phi$  as a function of density with that given by Equation 5 at a constant  $\phi = 0.9$ .  $E_{PU}$  is taken to be 2.5 GPa.

### Collapse Stress

The dependence of the plateau stress on foam density has also been address by Gibson and Ashby[7,8]. When a cellular solid is loaded in compression, the cell walls first flex as shown in Figure 15. When the vertical load in Figure 15 is small, the compressed columns that comprise the cell struts parallel to the applied load are laterally stable. As the load is increased, the column becomes unstable and this instability is termed “lateral buckling” and the applied load necessary to cause it is called the “Euler buckling load”. The derivation of the Euler buckling load is a well known problem in mechanics [13] and, when incorporated into the geometric model of Gibson and Ashby, can be used to predict the mechanical collapse of a foam as:

$$\frac{\sigma_c^*}{E_s} \approx C \times \left( \frac{\rho^*}{\rho_s} \right)^2 \left( 1 + \left( \frac{\rho^*}{\rho_s} \right)^{1/2} \right)^2 \quad (7)$$

where the constant, C, contains all of the physical and geometric factors relevant to the foam polymer and structure. In principle, C can be explicitly calculated. However, it is more expedient

to fit the measured collapse stress data shown in Figure 11 to Equation 7, using C as a fitting parameter. As shown in Figure 20, Equation 7 best fits the data for C = 0.02. As for the modulus prediction, the prediction derived by Gibson and Ashby for the collapse stress accurately reflects the density dependence of the foam over the range of densities measured.

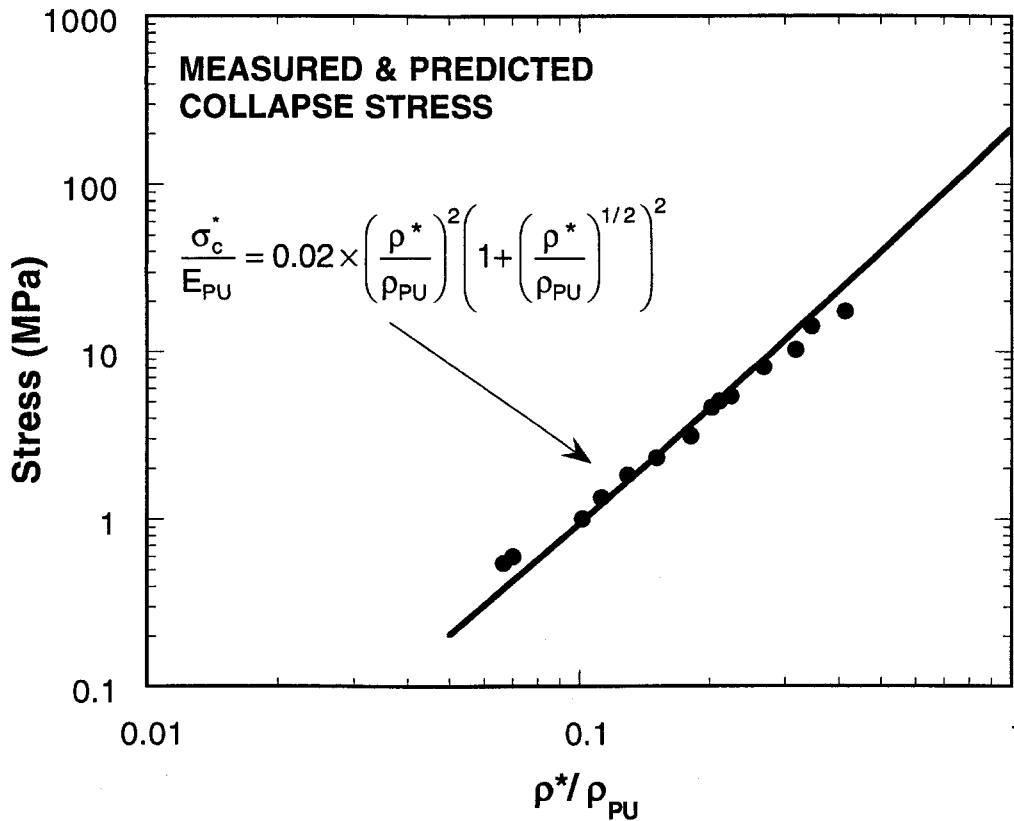


Figure 20. Comparison of collapse stress measurements to Equation 7 vs. normalized density.

### Prediction of Powder-Filled Foam Properties

The strut of a particulate-filled polyurethane foam is essentially a polymer-matrix composite consisting of two or more separate constituents, a continuous matrix phase and a discontinuous filler phase, which are combined to optimize designated properties of the composite structure. The change in properties of a particulate loaded foam (from that of an unloaded foam) should track with the effect of the additive on the properties of the monolithic polymer. Thus, it should be possible to predict the behavior of a particulate-filled foam by understanding the effect of the filler phase on the host matrix.

Much work has been done in regards to characterizing the effect of filler phases on the properties of resin matrix composites. Palumbo et. al. have studied the mechanical behavior of a composite consisting of a fully dense epoxy matrix and hollow glass microspheres (GMB) [14]. Results of this work revealed that the modulus of the composite decreased with increasing loading fraction of the GMB which has a lower modulus than the host epoxy matrix. In another study, Domeier et. al. found much the same effect in a similar epoxy/GMB composite system [15]. In contrast,

Monette et. al. observed an increase in Young's modulus when silica beads were dispersed throughout an epoxy matrix [16]. The experimental data revealed an increasing elastic modulus as the volume fraction of filler was increased. Similar findings were reported for an epoxy/alumina system [15]. In both instances, the modulus of the additives were greater than that of the matrix yielding composite structures of overall greater stiffness.

Beyond these experimental investigations, there have been many other studies [17,18] devoted to modeling the elastic properties of composites. The two most widely used methods for predicting the mechanical properties of particulate-reinforced composites are those developed by Hashin and Shtrikman [19] and Kerner [20].

In the latter case, a composite is considered to be a distribution of spherical particles suspended in a homogeneous matrix. The analysis assumes that there exists an average state of stress and strain within each particle when subjected to a hydrostatic stress. Kerner then calculated the bulk modulus of the composite ( $\kappa_c$ ) to be:

$$\kappa_c = \frac{\sum \frac{\kappa_f \theta_f}{3\kappa_f + 4\mu_m}}{\sum \frac{\theta_f}{3\kappa_f + 4\mu_m}} \quad (8)$$

where:  $\kappa_f$  is the bulk modulus of the filler phase,  $\theta_f$  = volume fraction of the filler and  $\mu_m$  is the shear modulus of the matrix solid.

To find the composite shear modulus ( $\mu_c$ ), Kerner considered the average effect of a uniform tension stress applied to the system and arrived at an expression for the shear modulus as:

$$\mu_c = \mu_m \frac{\sum \frac{\mu_f \theta_f}{(7-5\nu_m)\mu_m + (8-10\nu_s)\mu_f} + \frac{\theta_m}{15(1-\nu_m)}}{\sum \frac{\mu_s \theta_f}{(7-5\nu_s)\mu_m + (8-10\nu_m)\mu_f} + \frac{\theta_m}{15(1-\nu_m)}} \quad (9)$$

where  $\mu_f$  is the shear modulus of the filler,  $\theta_m$  = volume fraction of the matrix, and  $\nu_m$  = Poisson's ratio of the matrix.

The resulting Kerner equations are quite complicated and can be difficult to apply. Consequently, Halpin and Tsai [21-23] have shown that by grouping terms which pertain to the Poisson effect and particle geometry and also separating terms which depend on the elastic properties of the constituents, the Kerner equations can be generalized to the form:

$$\frac{M_c}{M_m} = \frac{1 + AB\theta_f}{1 - B\theta_f} \quad (10)$$

where  $M_c$  and  $M_m$  = any composite and matrix moduli.

$$A = \frac{7 - 5v_m}{8 - 10v_m} \quad (11)$$

and

$$B = \frac{(M_f/M_m) - 1}{(M_f/M_m) + A} \quad (12)$$

respectively.

Specifically for the Young's modulus of a particle strengthened composite:

$$E_c = E_m \left[ \frac{1 + AB\theta_f}{1 - B\theta_f} \right] \quad (13)$$

The measured moduli of monolithic composites have been compared favorably with predictions based on Equation 13 [14,15].

#### ***Modulus for Al-Loaded CRETE***

It has been shown that the Al powder is uniformly incorporated into the cell strut and cell wall elements of the foam. Therefore, these elements of the foam structure can be modeled as a composite with a matrix phase of solid polyurethane and a reinforcing phase of Al powder. As such, it should be possible to use the Halpin-Tsai equation (Eq. 13) in conjunction with the Gibson and Ashby model (Eq. 5) for the modulus of a closed-cell foam to predict the modulus of the Al-filled CRETE. In this case, the matrix modulus,  $E_m$  is the modulus of solid polyurethane,  $E_{PU}$ .  $E_c$  then represents the modulus of the filler-loaded strut (i.e., the composite) and is substituted for  $E_s$  (modulus of the foam strut material). In an analogous fashion,  $\rho_s$  is now the density of the PU-Al powder composite at each loading fraction of aluminum and is termed,  $\rho_{comp}$ . Finally,  $\rho^*$  is replaced by the total aggregate density of a specimen,  $\rho_{sample}$ . These new terms for the modulus and density of the PU-Al powder composite and specimens can be substituted in the expression:

$$E^* \approx E_s \phi^2 \left( \frac{\rho^*}{\rho_s} \right)^2 + (1 - \phi) \left( \frac{\rho^*}{\rho_s} \right) \quad (5)$$

The final governing expression for the modulus of the powder-loaded PU foam is then given as:

$$E^* \approx E_{PU} \phi^2 \left[ \frac{1 + AB\theta_f}{1 - B\theta_f} \right] \left[ \left( \frac{\rho_{sample}}{\rho_{comp}} \right)^2 + (1 - \phi) \left( \frac{\rho_{sample}}{\rho_{comp}} \right) \right] \quad (14)$$

Substituting appropriate values into Equations 11 and 12, the parameters A and B can be calculated. This was accomplished by once again taking the modulus of solid polyurethane to be 2.5 GPa, and the modulus of aluminum to be 68.9 GPa [24]. Poisson's ratio for polyurethane

was taken as 0.35 [25] and the partitioning factor,  $\phi$ , was once again held constant at 0.9. The result of applying the final governing expression (Eq. 14) for the modulus of the aluminum loaded foam to the experimental data is shown in Figure 21.

Figure 21 compares the experimentally measured moduli to the predicted moduli for Al-loaded foam. The data for the aluminum filled foam is the same as that previously presented in Figure 14. The solid line represents the modulus values predicted by Equation 5 for the unfilled CRETE. The data points have been omitted for clarity. The additional traces show the predicted density dependence of the modulus from Equation 14 for each loading fraction of aluminum. Note that both the data and the prediction for the 5 wt. % aluminum samples are not presented since both show little change.

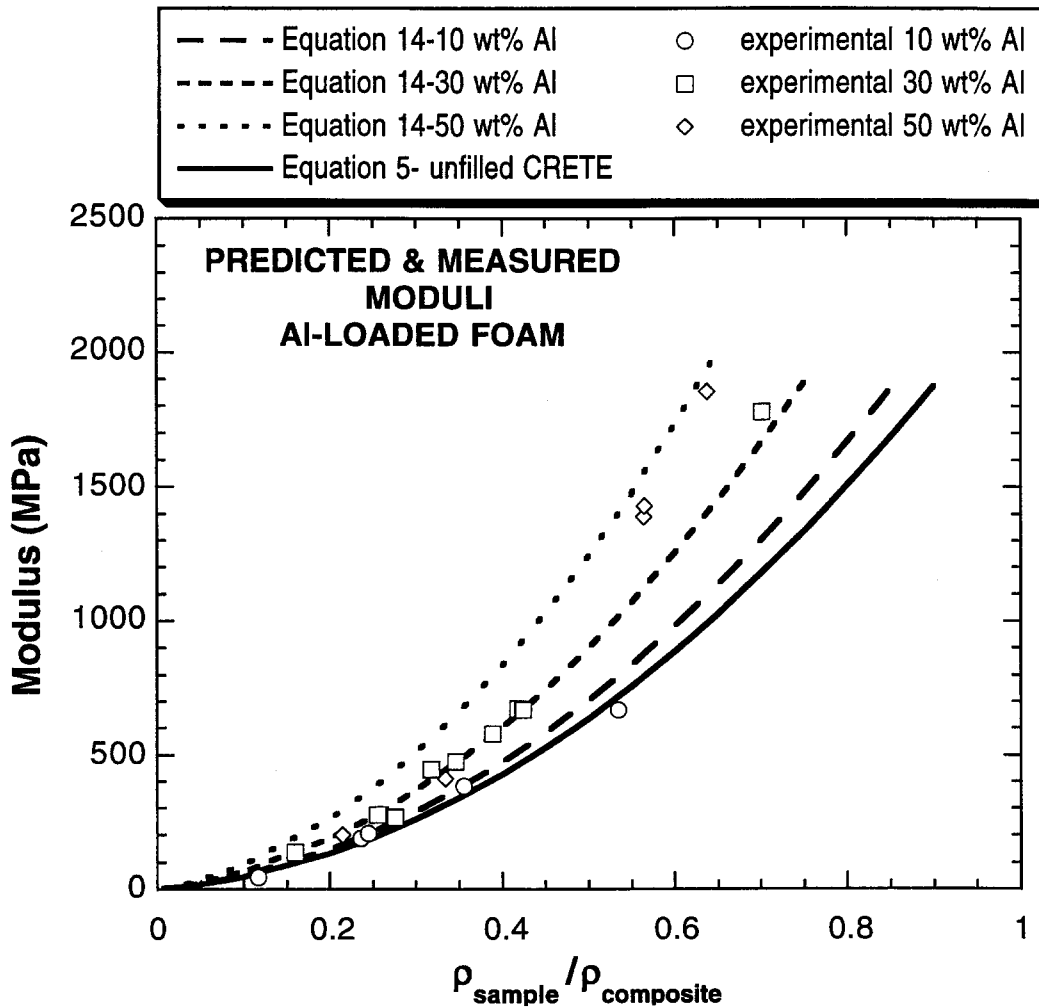


Figure 21. Combined Halpin-Tsai and Gibson and Ashby predictions for the modulus of Al powder-filled foam.

It is seen that the final governing equation captures the effect of the aluminum powder on the foam modulus quite well. The combined Halpin-Tsai form of the Kerner equation and Gibson and Ashby model accurately predicts the density dependence of the modulus as well as the increase in

modulus for each loading fraction. It accurately predicts that there is little effect on foam modulus for low (5 and 10 weight percent) loading fractions of aluminum. The trace corresponding to the 50 wt. % loading fraction appears to slightly overestimate the actual measured moduli. We suspect that this is due to the lack of complete bonding between the Al powder and the polymer matrix. This incomplete bonding reduces the effectiveness of the additive in stiffening the foam and as has been shown, promotes early fracture in highly loaded specimens.

***Collapse Stress for Al-Loaded CRETE***

Equation 7 indicates that the collapse stress should vary as a linear function of the modulus of the strut and cell wall material for foams of constant density. By combining Equations 7 and 13, the predicted collapse stress:

$$\sigma_c^* = 0.02 \times E_{PU} \left[ \frac{1 + AB\theta_f}{1 - B\theta_f} \right] \left( \frac{\rho^*}{\rho_{comp}} \right)^2 \left( 1 + \left( \frac{\rho^*}{\rho_{comp}} \right)^{1/2} \right)^2 \quad (15)$$

should track with the data shown in Figure 13. Such a comparison is shown in Figure 22 where the data points represent the measured collapse stress values from Figure 13 and the trace represents the expected collapse stress based on Equation 15.

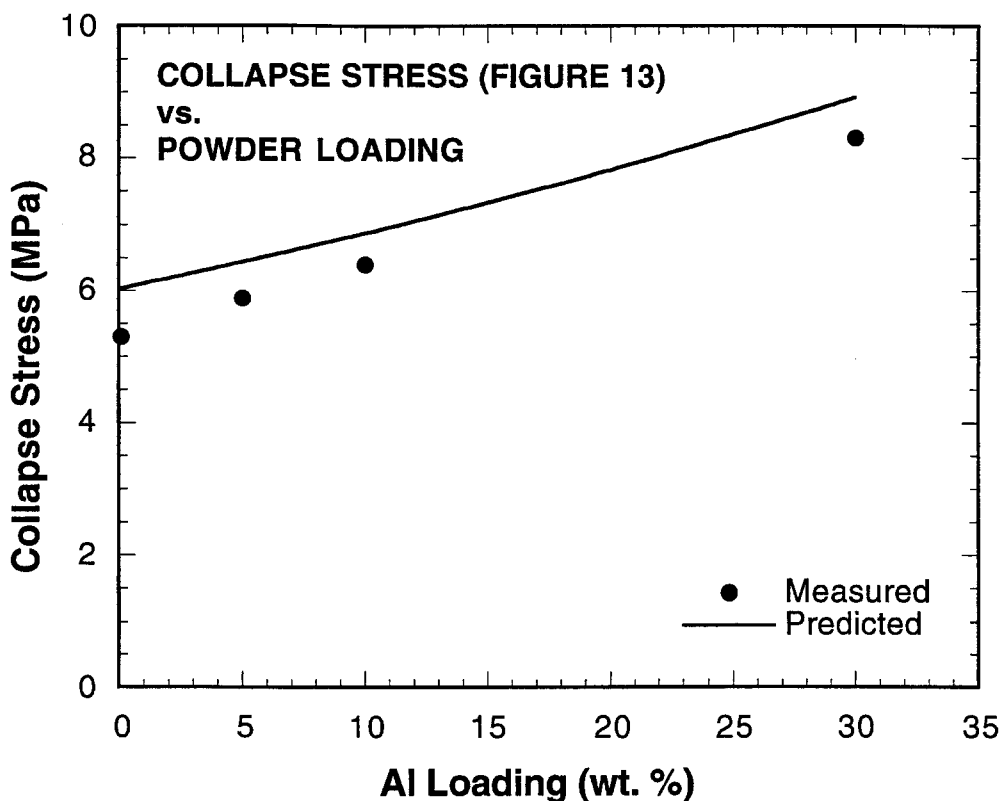


Figure 22. Comparison of combined Halpin-Tsai and Gibson and Ashby predictions for the collapse stress of a powder-loaded foam.

## V. Conclusion

Scanning electron microscopy revealed that the foam structure was uniform with respect to cell size and shape. Addition of aluminum powder did not alter the uniformity of the foam structure. A random non-agglomerated distribution of aluminum powder throughout the cell struts and walls was evident.

The modulus of the unfilled CRETE foam was increased with the addition of aluminum powder. The experimental data tended to group by loading fraction with 5 and 10 wt. % additions showing only minor increases in modulus. However, as the concentration of filler was increased to 30 and 50 wt. %, the foam modulus increased significantly. A 2 to 3-fold increase in modulus was realized at the highest loading fractions examined in this study. The density dependence of the modulus was unaffected by the additions of the filler phase. Over the range of densities examined, the strength of the filled foam was greater than that of the unfilled foam for all loading fractions of aluminum. However, high loading fractions caused the foam to be susceptible to cracking. This was the result of the poor adhesion between the aluminum powder and the polyurethane matrix. Consequently, ductility was decreased at high fractions of filler.

For the unfilled foam, the agreement between the measured modulus and the collapse stress with those predicted by Equations 5 and 7 suggests that a model available in the literature and based on a simple, idealized cell geometry can be useful in describing certain important mechanical and physical properties of encapsulant foams. By considering the strut of the filled foam to be a composite consisting of a rigid phase within a polyurethane matrix, the increase in the modulus and strength of the Al-loaded foam could be understood. A well known expression that describes the effect of rigid, spherical additives on the modulus of monolithic composites was incorporated into the Gibson and Ashby foam model. By combining these two models, expressions that accounted for both the composite nature of the polymer/powder solid and the overall foam structure were created. These expressions were shown to predict the effect of a rigid filler phase on both the modulus and strength of the loaded foam.

## **VI. Acknowledgement**

The authors wish to acknowledge the assistance of Mike Tootle (8712) for his help in sample preparation and testing, Nancy Yang and Eric Kleinschmidt (8715) for microscopy support and Craig Henderson (8230) for the original formulation of CRETE.

## VII. References

1. D. Klemmner and K. C. Frisch, *Handbook of Polymer Foams and Foam Technology*, (1991), Oxford University Press, N. Y.
2. W. R. Even, *private communication*, (1998), Sandia National Labs, C. A.
3. S. K. Bhattachara, *Metal-Filled Polymers: Properties and Applications*, pp. 5- 15, 172, (1986), Marcel Dekker, Inc., N. Y.
4. S. H. Goods, C. L. Neuschwanger, C. Henderson and D. M. Skala, *J. Appl. Polymer Sci.*, 68:1045 (1998).
5. W. F. Roff and J. R. Scott, *Fibers, Films, Plastics and Rubbers-A Handbook of Common Polymers*, p. 445, (1971), Butterworths, London.
6. E. E. Underwood, *Quantitative Stereology*, (1970), Addison-Wesley Publishing Company, Inc. Reading, , MA
7. L. J. Gibson and M. F. Ashby, *Proc. Roy. Soc.*, A382:43 (1982).
8. L. J. Gibson and M. F. Ashby, *Cellular Solids, Structure and Properties*, (1988), Pergamon Press, N. Y.
9. *Plastics Digest*, Vol.2, D.A.T.A., Englewood, CO., 1994, p1301-1304
10. M. R. Patel and I. Finnie, *J. Mater.*, 5:909 (1970).
11. R. M. Christensen, *J. Meck. Phys. Solids*, 34, 563 (1968)
12. D. W. Reitz, M. A. Schuetz and L. R. Glicksman, *J. Cell. Plast.*, 20:104 (1984).
13. S. Timoshenko and D. H. Young, *Elements of Strength of Materials*, 4th Ed., p. 212, 342, (1962) D. van Nostrand & Co. Inc., N. Y.
14. M. Palumbo, G. Donzella, E. Tempesti and P Ferruti, *J. Appl. Polymer Sci.*, 60, 47-53, (1996)
15. L. Domeier, D. M. Skala, S. H. Goods, C. L. Neuschwanger, M. L. Tootle and W. Lu, *National Technical Information Service*, UC-404 (1998).
16. L. Monette, M. P. Anderson, H. D. Wagner and R. R. Mueller, *J. Appl. Phys.*, 75:1442 (1994).
17. B. Paul, *AIME Trans.*, 218:36 (1960).
18. R. D. Bohme, *J. Appl. Polymer Sci.*, 12:1097 (1968).
19. Z. Hashin and S. Shtrikman, *J. Mech. Phys. Solids*, 11:127 (1963).

20. E. H. Kerner, *Proc. Phys. Soc.*, **B69**:808 (1956).
21. J. C. Halpin, *J. Comp. Mater.*, **3**:732 (1969).
22. J. C. Halpin, *Primer on Composite Materials Analysis*, 2nd Ed., p. 161, (1992) Technomic Publishing, P. A.
23. S. W. Tsai, *U. S. Government Rep.*, AD 834851, (1968).
24. Smithells, C.J. and E.A. Brandes, *Metals Reference Book*. 5th ed. 1976, Woburn, MA: Butterworths.
25. A. W. Birley, B. Haworth and J. Batchelor, *Physics of Plastics- Processing, Properties*.

**DISTRIBUTION:**

5                   Hewlett-Packard Company  
                    Attn: Cari Neuschwanger  
                    1501 Page Mill Road, MS 5L-C  
                    Palo Alto, CA 94304-1126

1                   Atomic Weapons Establishment  
                    Attn: Norman R. Godfrey  
                    Aldermaston  
                    Reading, Berks  
                    England RG74PR  
                    UNITED KINGDOM

1           MS 0367       P. B. Rand, 1815

1           MS 0367       R. S. Saunders, 1815

1           MS 0443       M. K. Neilsen, 9117

1           MS 0834       M. L. Hobbs, 9112

1           MS 0834       A. M. Kraynik, 9112

1           MS 0928       C. J. Adkins, 1472

1           MS 0958       M. W. Donnelly, 1472

1           MS 0958       J. A. Emerson, 1472

1           MS 0958       T. R. Guess, 1472

1           MS 0958       R. L. Myers, 1472

1           MS 0961       J. A. Sayre, 1403

1           MS 1407       R. J. Salzbrenner, 1805

1           MS 1407       T. A. Ulibarri, 1811

1           MS 1407       J. H. Aubert, 1815

1           MS 9001       M. E. John, 8000  
                    Attn: R. C. Wayne, 2200, MS 9005  
                    M. E. John, 8100 (A), MS 9004  
                    W. J. McLean, 8300, MS 9054  
                    R. C. Wayne, 8400 (A), MS 9007  
                    P. N. Smith, 8500, MS 9002  
                    P. E. Brewer, 8600, MS 9031  
                    L. A. Hiles, 8800, MS 9031  
                    D. R. Henderson, 8900 (A), MS 9003

1           MS 9042       W. Y. Lu, 8746

1           MS 9102       M. W. Perra, 8402

1           MS 9403       M. I. Baskes, 8712

10          MS 9403       S. H. Goods, 8712

1           MS 9403       M. L. Tootle, 8712

1	MS 9405	T. M. Dyer, 8700 Attn: C. M. Hartwig, 8701, MS 9405 J. C. F. Wang, 8713, MS 9403 G. J. Thomas, 8715, MS 9402 K. L. Wilson, 8716, MS 9042 S. M. Foiles, 8717, MS 9042 E.-P. Chen, 8742, MS 9042 P. E. Nielan, 8743, MS 9405 W. A. Kawahara, 8746, MS 9042
1	MS 9405	L. Domeier, 8230
1	MS 9405	C. Henderson, 8230
1	MS 9405	J. M. Hruby, 8230
1	MS 9405	D. Irvin, 8230
1	MS 9405	P. Kiefer, 8230
1	MS 9405	D. Skala, 8730
10	MS 9405	L. Whinnery, 8230
1	MS 9420	L. A. West, 8200 (A) Attn: B. Affeldt, 8210, MS9133 C. Oien, 8260, MS 9409 G. Kubiak, 8250, MS 9409 A. J. West, 8240, MS 9430 L. N. Tallerico, 8204, MS 9430
3	MS 9018	Central Technical Files, 8940-2
1	MS 0899	Technical Library, 4916
1	MS 9021	Technical Communications Dept., 8815/Technical Library, MS0899, 4916
1	MS 9021	Technical Communications Dept. 8815, for DOE/OSTI